Vehicle System Dynamics

ISSN: 0042-3114 (Print) 1744-5159 (Online) Journal homepage: http://www.tandfonline.com/loi/nvsd20

A design methodology for mechatronic vehicles: application of multidisciplinary optimization, multibody dynamics and genetic algorithms

Y. He & J. McPhee

To cite this article: Y. He & J. McPhee (2005) A design methodology for mechatronic vehicles: application of multidisciplinary optimization, multibody dynamics and genetic algorithms, Vehicle System Dynamics, 43:10, 697-733, DOI: 10.1080/00423110500151077

To link to this article: http://dx.doi.org/10.1080/00423110500151077

Published online: 16 Feb 2007.

Submit your article to this journal

Article views: 230

View related articles

Citing articles: 9 View citing articles

Full Terms & Conditions of access and use can be found at
http://www.tandfonline.com/action/journalInformation?journalCode=nvsd20

Download by: [Kungliga Tekniska Hogskola] **Date:** 26 November 2015, At: 04:36

Vehicle System Dynamics
Vol. 43, No. 10, October 2005, 697–733

Taylor & Francis
Taylor & Francis Group

A design methodology for mechatronic vehicles: application of multidisciplinary optimization, multibody dynamics and genetic algorithms

Y. HE† and J. McPHEE*‡

†Mechanical Engineering, University of Waterloo, 200 University Avenue West, Waterloo, Ontario, Canada N2L 3G1
‡Systems Design Engineering, University of Waterloo, 200 University Avenue West, Waterloo, Ontario, Canada N2L 3G1

Downloaded by [Kungliga Tekniska Hogskola] at 04:36 26 November 2015

A design methodology for mechatronic vehicles is presented. With multidisciplinary optimization (MDO) methods, strongly coupled mechanical, control and other subsystems are integrated as a synergistic vehicle system. With genetic algorithms (GAs) at the system level, the mechanical, control and other relevant parameters can be optimized simultaneously. To demonstrate the feasibility and efficacy of the proposed design methodology for mechatronic vehicles, it is used to resolve the conflicting requirements for ride comfort, suspension working spaces and unsprung mass dynamic loads in the optimization of half-vehicle models with active suspensions. Both deterministic and random road excitations, both rigid and flexible vehicle bodies and both perfect measurement of full state variables and estimated limited state variables are considered. Numerical results show that the optimized vehicle systems based on the methodology have better overall performance than those using the linear quadratic Gaussian (LQG) controller. It is shown that the methodology is suitable for complex design optimization problems where: (1) there is interaction between different disciplines or subsystems; (2) there are multiple design criteria; (3) there are multiple local optima; (4) there is no need for sensitivity analysis for the optimizer at the system level; and (5) there are multiple design variables.

Keywords: Mechatronic vehicles; Multidisciplinary optimization; Multibody dynamics; Genetic algorithms

1. Introduction

Conventionally, in the design of robots, airplanes and ground vehicles, a common practice has been a sequential approach, such that passive mechanical subsystems are designed first and active control subsystems are added subsequently [1–3]. The resultant design may behave less 'optimally' overall due to the mechanical and control parameters not being simultaneously considered as design variables. Since there are inherent couplings among the passive and active subsystems, it is expected that an integrated control and mechanical design process may coordinate the different or conflicting requirements from the mechanical and control subsystems so as to achieve an optimal behaviour of the overall systems.

*Corresponding author. Email: mcphee@real.uwaterloo.ca

Vehicle System Dynamics
ISSN 0042-3114 print/ISSN 1744-5159 online © 2005 Taylor & Francis
http://www.tandf.co.uk/journals
DOI: 10.1080/00423110500151077

In a robot design, Pil *et al.* [1] have proposed a recursive experimental optimization method for simultaneously optimizing both the mechanical structure and controller of the mechatronic system. In the design, the mechanical structure might be modified recursively and quickly with structure reinforcement and rapid prototyping techniques. The feedback control gains were adjusted with the mechanical structure modification and this procedure was iterated until the design criteria were reached.

In the design of a glider, it is shown [2] that a simultaneous optimization of aerodynamics, structures and control is more efficient than the corresponding sequential approach. The inadequacy of the sequential approach to the optimization motivates the application of multidisciplinary optimization (MDO) to the simultaneous design of a structure and a control system to achieve the active flutter suppression.

In the design of road vehicles, Bestle *et al.* [3–5] have recommended that an integrated modelling and control design be performed to improve the performance of suspension systems and that parameters of both active and passive elements be adjusted adequately to attain the optimal behaviour of the overall vehicle. Baumal *et al.* [6, 7] have applied a design method using genetic algorithms to the optimization of both passive and active parameters for both road and rail vehicles with active suspensions. However, these researchers have limited their control strategies to the use of 'skyhook' dampers [8] in their design optimizations. Since the 1970s, the optimal control theory has been widely used in designing controllers for active suspensions. Thompson [9, 10] applies the optimal linear state feedback method to the design of active suspensions based on both quarter-vehicle and half-vehicle models with deterministic road excitations. Hac [11, 12] uses the linear quadratic Gaussian (LQG) optimal control method for deriving active suspensions based on both quarter-vehicle and half-vehicle models with random road excitations.

To introduce the well-known linear quadratic Gaussian (LQG) controller [10, 12] and Kalman estimator [12] into the design of mechatronic vehicles, He and McPhee [13, 14] proposed an integrated mechanical and control method for the optimization of vehicles with active suspensions based on a 2 degree of freedom (DOF) quarter-vehicle model. In fact, their approach is an application of a multidisciplinary optimization method to the design of road vehicles. The integrated method was implemented in a GA-A'GEM-MATLAB simulation environment in such a way that the linear mechanical vehicle model is designed in a multibody dynamics software package, i.e. A'GEM [15], the controllers and estimators are constructed using the LQG and Kalman filter algorithms in Matlab, then the combined mechanical and control model is optimized simultaneously using a genetic algorithm (GA). However, the resulting optimal controllers, estimators and mechanical subsystems were based on quarter-vehicle models [14]. Applied to a complex vehicle model, such controllers may behave less optimally because no provision for pitch or roll motions can be made in the quarter-vehicle models [16].

The purpose of this study is to extend the work reported in [14] by: (1) proposing a more general framework of a design methodology for mechatronic vehicles, which may contain anti-lock braking systems (ABS), active suspension systems, active steering systems and other control subsystems or a combination of these units; (2) determining if this methodology could be applied to more realistic mechatronic half-vehicle models instead of the simple quarter-vehicle models.

In this methodology, we intend to use multidisciplinary optimization methods to integrate strongly coupled mechanical, control and other subsystems as a synergistic vehicle system. To simultaneously optimize the mechanical, control and other relevant subsystems or disciplines, a GA will be introduced at the system level and effective algorithms at the subsystem level. To demonstrate the efficacy of the methodology, it is used to resolve the conflicting requirements for ride comfort, suspension working spaces and unsprung mass dynamic loads in the design optimization of the half-vehicle models with active suspensions. Both deterministic and

Downloaded by [Kungliga Tekniska Hogskola] at 04:36 26 November 2015

random road excitations, both rigid and flexible vehicle body and both perfect measurement of full state variables and estimated limited state variable are considered.

Recently, in the design of controllers for active suspensions, nonlinear effects of vehicle system models have often been taken into account [17]. However, in the optimal suspension control synthesis and analysis, linear vehicle system models are frequently used [18]. This optimal suspension control synthesis and analysis serves as a precursor necessary to provide the overall trends and desired designs. Once a candidate suspension has been established in this way, further evaluation would typically proceed via more refined and complex models including various nonlinear effects. Moreover, linear vehicle system models are well-suited for applications of the LQG optimal control technique. Thus, in the application of our methodology, two linear half-vehicle models are used.

In the following sections, first, the design methodology for mechatronic vehicles is presented; then this methodology is applied to the design optimization of the half-vehicle models with active suspensions.

Downloaded by [Kungliga Tekniska Hogskola] at 04:36 26 November 2015

2. A design methodology for mechatronic vehicles

A successful mechatronic vehicle system design requires harmonization of a number of criteria and constraints. Such a design problem can be modelled as a constrained optimization in the design variable space. However, for such optimization, due to its dimensionality (*e.g.* the number of active and passive design variables), complexity (*e.g.* a combination of mechanical, hydraulic, control and other subsystems) and expense for analysis, a decomposition approach is recommended so as to enable concurrent execution of smaller and more manageable tasks [19]. To preserve the couplings that naturally occur among the subsystems of the whole problem, such optimization by various types of decomposition must include a degree of coordination at the system and subsystem levels. Multidisciplinary optimization (MDO) offers effective methods for performing the above optimization so as to resolve the trade-off relations among the various design criteria at the system and subsystem levels. Therefore, based on the above MDO principle, a general framework of a design methodology for mechatronic vehicles is proposed.

2.1 *The proposed framework*

The proposed framework for the design of mechatronic vehicles is shown in figure 1. To generate objective-oriented vehicle system models, $M_1, M_2, \ldots, M_n$, the effective dynamic system modelling technique (multibody dynamics) is utilized. For instance, in the development of mechatronic vehicles with slip control, active steering and active suspension control, respectively, the objective-oriented vehicle models may be longitudinal, lateral and vertical vehicle dynamic models accordingly, or a combination of the three. Based on the features of vehicle systems to be optimized, a variety of successful computer programs for multibody systems, e.g. ADAMS, SIMPACK, VAMPIRE and A'GEM, could be used for this purpose.

In the design of vehicles, relevant hydraulic subsystems, $H_1, H_2, \ldots, H_q$, can be modelled based on fluid mechanics. For example, to consider aerodynamic effects on high speed road vehicles, the computational fluid dynamic (CFD) modelling technique may be utilized; to model hydraulic actuators for mechatronic vehicles, relevant hydraulic power control approaches may be applied.

For a specified mechatronic vehicle design, relevant subsystems, $A_1, A_2, \ldots, A_m$, such as controllers and estimators, can be introduced. In the case of an integrated vehicle control system

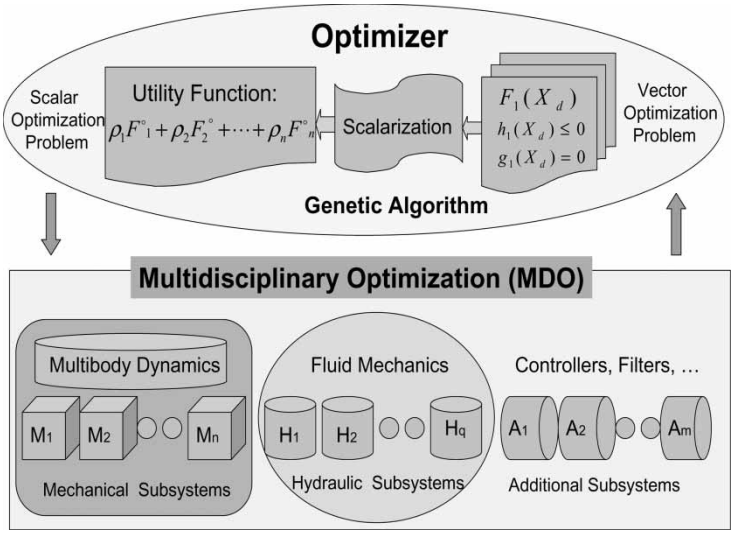

Figure 1. Proposed framework for the design optimization of mechatronic vehicles.

Downloaded by [Kungliga Tekniska Hogskola] at 04:36 26 November 2015

including slip control, active steering and active suspension control, the relevant subsystems may be controllers and estimators for ABS, active steering and active suspension subsystems.

By means of multidisciplinary optimization formulations, the above strongly coupled subsystems or disciplines are integrated as a synergistic mechatronic vehicle system.

With the integration of these multiple subsystems to be optimized, at the system level one is faced with a vector optimization problem with a set of design criteria, $\mathbf{F}(\mathbf{X}_d)$, where $\mathbf{X}_d$ is a vector of design variables and corresponding constraints, $\mathbf{g}(\mathbf{X}_d) = \mathbf{0}$ and $\mathbf{h}(\mathbf{X}_d) \le \mathbf{0}$.

In a dynamic system design such as the one considered here, an effective approach is to reduce the vector optimization problem to a single or a sequence of scalar nonlinear programming problems using the technique of scalarization or hierarchization [20, 21]. Then, the scalar optimization problem may be solved by existing algorithms such as gradient-based local search methods and global search stochastic algorithms. However, when the gradient-based local search algorithms, e.g. sequential quadratic programming (SQP), are applied to the reduced scalar optimization problem, the main problems are [21]: (1) loss of guarantee for Pareto optimality due to the convergence to local optima; (2) failure to compute the whole Pareto set in the case of non-convex problems; and (3) difficulty to get a clear impression on the whole Pareto set in any case.

In contrast, with the use of global search stochastic algorithms, e.g. simulated annealing algorithms (SAs) [20] and genetic algorithms [7, 22], a much clearer picture of the Pareto set can be obtained for the reduced optimization problem using the scalarization technique. This whole Pareto set can be derived using several sets of weighting factors and post-processing the corresponding sampled points (offered by the stochastic algorithms) from the design space. Thus, in the methodology, the scalarization technique is adopted to convert the vector optimization problem into a scalar one and a GA is applied for finding the solutions to the scalar optimization problem.

The resulting utility function takes the form of $\rho_1 F_1^\circ + \rho_2 F_2^\circ + \cdots + \rho_n F_n^\circ$ (where ρ_i, $i = 1, \ldots, n$, are weighting factors). Note that the term F_i° considers the original design criteria $F_i(\mathbf{X}_d)$ and corresponding constraints $\mathbf{g}_i(\mathbf{X}_d) = \mathbf{0}$ and $\mathbf{h}_i(\mathbf{X}_d) \le \mathbf{0}$.

The GA is used as the optimizer to resolve trade-off relations among various design criteria at the system level. Compared with local search algorithms such as gradient-based algorithms,

genetic algorithms have the distinguished properties of having higher reliability for finding the global optima, requiring no gradient information, using probability rules to guide their searches and being suitable for solving complex real-world problems. The detailed information about the GA used in the study will be described in detail in section 4.

The framework of the methodology consists of the main components: application of MDO methods, multicriteria optimization approaches, multibody dynamics, fluid mechanics, genetic algorithms, control theory and other techniques. The relevant multicriteria optimization approaches were described in detail by He and McPhee [22]. In the following subsection, a widely used MDO formulation method, All-in-One (A-i-O), is outlined.

Downloaded by [Kungliga Tekniska Hogskola] at 04:36 26 November 2015

2.2 *All-in-one formulation method*

Several MDO formulation methods exist, including the All-in-One (A-i-O) method that is commonly used for the solution of MDO problems. The A-i-O method is also known as the Multidisciplinary Feasibility (MDF) method [23]. When this method is used, the optimization problem can be formulated in the following general format:

$$\begin{cases} \text{minimize} & \mathbf{F}(\mathbf{X}_d, \mathbf{U}(\mathbf{X}_d)) \\ \text{with respect to} & \mathbf{X}_d \\ \text{subject to} & \begin{cases} \mathbf{g}(\mathbf{X}_d, \mathbf{U}(\mathbf{X}_d)) \le \mathbf{0} \\ \mathbf{C}_l \le \mathbf{X}_d \le \mathbf{C}_u \end{cases} \end{cases} \tag{1}$$

where

$$\begin{cases} \mathbf{U}(\mathbf{X}_d) = \mathbf{A}(\mathbf{X}_d, \mathbf{Y}) \\ \mathbf{Y} = \mathbf{G}(\mathbf{X}_d, \mathbf{U}(\mathbf{X}_d)) \end{cases} \tag{2}$$

and $\mathbf{C}_u$ and $\mathbf{C}_l$ are the upper and lower bounds on the design variables $\mathbf{X}_d$, $\mathbf{U}(\mathbf{X}_d)$ is the system output variable vector, $\mathbf{A}(\mathbf{X}_d, \mathbf{Y})$ is the analysis mapping from the inputs $\mathbf{X}_d$ and $\mathbf{Y}$ of an analysis discipline to the outputs $\mathbf{U}$, $\mathbf{G}(\mathbf{X}_d, \mathbf{U}(\mathbf{X}_d))$ is the mapping to the inputs required for an analysis discipline from the output of another analysis discipline and $\mathbf{F}(\mathbf{X}_d, \mathbf{U}(\mathbf{X}_d))$ and $\mathbf{g}(\mathbf{X}_d, \mathbf{U}(\mathbf{X}_d))$ are the objective function vector and constraints, respectively. Note that $\mathbf{g}(\mathbf{X}_d, \mathbf{U}(\mathbf{X}_d))$ may also contain equality constraints.

Figure 2 shows the data flow in an A-i-O optimization of a problem involving two analysis disciplines. The system consists of an optimizer that controls specified objective $\mathbf{F}$ and constraints $\mathbf{g}$, discipline 1 with analysis solver $\mathbf{A}_1$ and discipline 2 with analysis solver $\mathbf{A}_2$. For a certain iteration in the outer optimization loop, the fixed design variable vector $\mathbf{X}_d$ is provided by the optimizer to the coupled analysis disciplines. Then in the interior loop, a complete

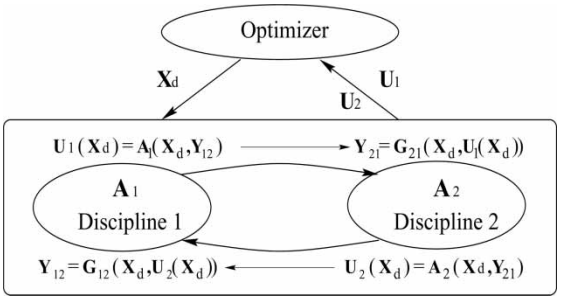

Figure 2. All-in-One (A-i-O) method.

discipline 1 analysis and discipline 2 analysis is performed with that value of $\mathbf{X}_d$ to obtain system output variable vectors $\mathbf{U}_1(\mathbf{X}_d)$ and $\mathbf{U}_2(\mathbf{X}_d)$. Note that this interior loop analysis may also be iterative. The output variable vectors $\mathbf{U}_1(\mathbf{X}_d)$ and $\mathbf{U}_2(\mathbf{X}_d)$ are used for evaluating the objective $\mathbf{F}(\mathbf{X}_d, \mathbf{U}_1(\mathbf{X}_d), \mathbf{U}_2(\mathbf{X}_d))$ and constraints $\mathbf{g}(\mathbf{X}_d, \mathbf{U}_1(\mathbf{X}_d), \mathbf{U}_2(\mathbf{X}_d))$.

In Figure 2, the interdisciplinary mapping $\mathbf{G}_{ij}$ means that given the output variable vector $\mathbf{U}_j$ from discipline j, a suitable variable vector $\mathbf{Y}_{ij}$ can be calculated for use by discipline i. We say that we have single discipline feasibility for discipline i when the solver $\mathbf{A}_i$ has been executed successfully and solved for output variable vector $\mathbf{U}_i$, given the input variable vector $\mathbf{Y}_{ij}$. Here, 'feasibility' for a single discipline means that the equations the discipline code is intended to solve are satisfied. For this two analysis discipline case, the optimization problem can be rewritten as:

$$\begin{cases} \text{minimize} & \mathbf{F}(\mathbf{X}_d, \mathbf{U}_1(\mathbf{X}_d), \mathbf{U}_2(\mathbf{X}_d)) \\ \text{with respect to} & \mathbf{X}_d \\ \text{subject to} & \begin{cases} \mathbf{g}(\mathbf{X}_d, \mathbf{U}_1(\mathbf{X}_d), \mathbf{U}_2(\mathbf{X}_d)) \leq \mathbf{0} \\ \mathbf{C}_l \leq \mathbf{X}_d \leq \mathbf{C}_u \end{cases} \end{cases} \tag{3}$$

where

$$\begin{cases} \mathbf{U}_1(\mathbf{X}_d) = \mathbf{A}_1(\mathbf{X}_d, \mathbf{Y}_{12}) \\ \mathbf{U}_2(\mathbf{X}_d) = \mathbf{A}_2(\mathbf{X}_d, \mathbf{Y}_{21}) \\ \mathbf{Y}_{12} = \mathbf{G}_{12}(\mathbf{X}_d, \mathbf{U}_2(\mathbf{X}_d)) \\ \mathbf{Y}_{21} = \mathbf{G}_{21}(\mathbf{X}_d, \mathbf{U}_1(\mathbf{X}_d)) \end{cases} . \tag{4}$$

Notice that if a gradient-guided optimization algorithm is used to solve the above problem, a complete multidisciplinary analysis (MDA) is necessary not just at every iteration of the optimization loop, but at every point where the derivatives are to be evaluated. Thus, it is very expensive to attain multidisciplinary feasibility (i.e. simultaneous feasibility in all disciplines) in realistic applications.

To demonstrate the feasibility and efficacy of the proposed design methodology for resolving conflicting design requirements of mechatronic vehicles, the methodology is applied to the design of road vehicles with active suspensions.

3. Vehicle system models

Figure 3 shows the half-vehicle models to be optimized. Two different cases, i.e. rigid vehicle body with deterministic road inputs and flexible vehicle body with stochastic road inputs, are considered. In figure 3, the rigid vehicle body is represented by solid lines and the flexible one by curved dashed lines, respectively. The vehicle is assumed to have a longitudinal central plane of symmetry, so that M is half the body mass and I_c half the pitch moment of inertia about the centre of gravity of the body. For the rigid vehicle body, the motions considered are the body heave (x_5) and pitch (φ). In addition to the rigid body modes, for the flexible body case, the body structure is described by its first 3 bending modes. The natural frequencies and approximating functions of mode shapes are based on those used by Hac [12]. Thus, the flexible body is approximately modelled as a beam of stiffness EI, body cross section area A and mass density ρ. The front and rear unsprung masses are represented by rigid bodies of masses m_1 and m_2; they have a vertical DOF represented by x_1 and x_3, respectively. The actuator forces u_1 and u_2 are assumed to be applied between the unsprung masses and the vehicle body, at points A and B, respectively. In the secondary suspensions, k_1, k_2 , c_1 and

Downloaded by [Kungliga Tekniska Hogskola] at 04:36 26 November 2015

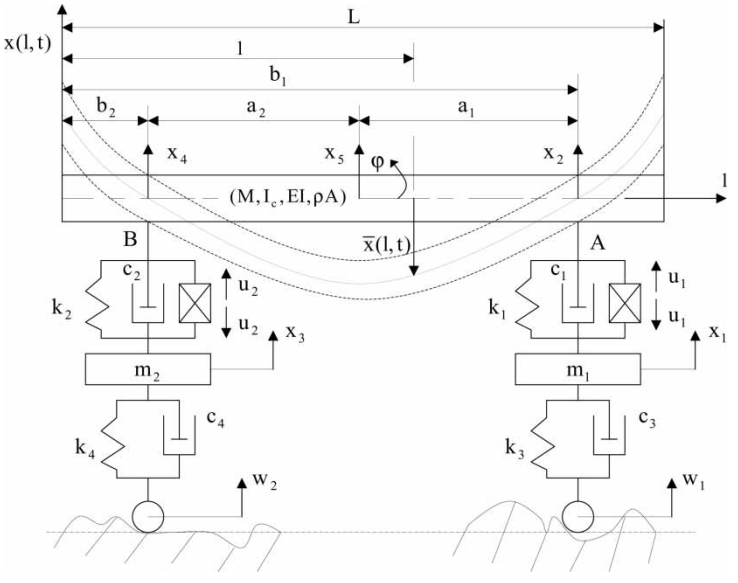

Figure 3. Half-vehicle models.

c_2 represent stiffness and damping ratios of passive front and rear elements; in the primary suspensions, k_3, k_4, c_3 and c_4 denote stiffness and damping ratios of passive front and rear elements. In motion, the front and rear primary suspensions are submitted, respectively, to the road displacement excitations w_1 and w_2.

The nominal system parameters are provided in the Appendix for both the half-vehicle models with rigid and flexible vehicle bodies. In the following subsections, the governing equations of motion for both the half-vehicle models are provided.

3.1 *Rigid vehicle body with deterministic road input case*

The dynamic equations of motion for the controlled vehicle model can be written as

$$\begin{cases} \dot{\mathbf{x}} = \mathbf{A}\mathbf{x} + \mathbf{B}\mathbf{u} + \mathbf{D}\dot{\mathbf{w}} \\ \mathbf{y} = \mathbf{C}\mathbf{x} \end{cases} \tag{5}$$

where the state variables $\mathbf{x}$, actuator forces $\mathbf{u}$, and road displacement excitations $\mathbf{w}$ are

$$\begin{cases} \mathbf{x} = [x_1 - w_1 \quad x_2 - w_1 \quad x_3 - w_2 \quad x_4 - w_2 \quad \dot{x}_1 \quad \dot{x}_2 \quad \dot{x}_3 \quad \dot{x}_4]^T \\ \mathbf{u} = [u_1 \quad u_2]^T \\ \mathbf{w} = [w_1 \quad w_2]^T \end{cases} . \tag{6}$$

The system, control, disturbance and output matrices, i.e. $\mathbf{A}$, $\mathbf{B}$, $\mathbf{C}$, and $\mathbf{D}$, are provided in the Appendix. Assuming the vehicle is travelling at a constant speed (V) and the two road inputs (w_1 and w_2) are separated by wheel base $a_1 + a_2$, we have the following relation

$$\begin{cases} w_1(t) = w_2(t + D) \\ D = (a_1 + a_2)/V \end{cases} . \tag{7}$$

Note that in the ride quality analysis for vehicles, the road profiles are often modelled as displacement spectral density functions with the characteristics of filtered white noise or

Downloaded by [Kungliga Tekniska Hogskola] at 04:36 26 November 2015

integrated white noise [26]. The first case is the random road input case that will be discussed in the following subsection. In the integrated white noise road input case, for a linear vehicle system, the mean-squared value of any output signal of interest is simply related to the integral-squared value of the corresponding output signal due to a unit step input. For a given velocity, if the system is optimal for a unit step input, it will also be optimal for the corresponding integrated white noise road input [10]. Since it is much simpler to generate a unit step function than a continuous random signal for the road inputs, here we assume that the road inputs w_1 and w_2 are unit step inputs.

3.2 *Flexible vehicle body with random road input case*

The road inputs w_1 and w_2 are assumed to be a filtered white noise process. The power spectral density (PSD) of the filtered white noise road displacement can be formulated as [12]

$$S_w(\omega) = (\sigma_t/\pi)a_t V/(\omega^2 + a_t^2 V^2) \tag{8}$$

where σ_t is the variance of road irregularities, a_t the road roughness constant, ω the temporal angular freguency and V the vehicle velocity. The process vector $\mathbf{w}$ can be generated from the pure white noise precess vector ξ using a shaping filter of the form

$$\dot{\mathbf{w}} = \mathbf{F}_w \mathbf{w} + \mathbf{D}_w \xi \tag{9}$$

where

$$\begin{cases} \mathbf{w} = [w_1 \quad w_2]^T \\ \xi = [\xi_1 \quad \xi_2]^T \\ \mathbf{F}_w = -a_t V \mathbf{I}_{2\times 2} \\ \mathbf{D}_w = \mathbf{I}_{2\times 2} \end{cases} \tag{10}$$

and $\mathbf{I}_{2\times 2}$ is identity matrix of dimension 2×2, ξ_1 and ξ_2 are zero mean white noise processes. Since the road inputs w_1 and w_2 also have the relation shown in (7), ξ_1 and ξ_2 are related by

$$\xi_1(t) = \xi_2(t + D). \tag{11}$$

Therefore, the Gaussian white noise process vector ξ, *i.e.* $[\xi_1 \quad \xi_2]^T$, has the covariance matrix taking the form as

$$\begin{cases} E[\xi(t)\xi^T(\tau)] = Q_0 \begin{bmatrix} \delta(t-\tau) & \delta(t-\tau+D) \\ \delta(t-\tau-D) & \delta(t-\tau) \end{bmatrix} \\ Q_0 = 2\sigma_t a_t V \end{cases} \tag{12}$$

where $\delta(\cdot)$ stands for the Dirac function. In our study, two different cases are considered. In the first case, the correlation between ξ_1 and ξ_2 is taken into account. In the second case, the correlation is neglected. If the correlation between ξ_1 and ξ_2 is neglected, the covariance matrix can be rewritten as

$$\begin{cases} E[\xi(t)\xi^{\mathbf{T}}(\tau)] = \mathbf{Q}\delta(t-\tau) \\ \mathbf{Q} = 2\sigma_t a_t V \mathbf{I}_{2\times 2} \end{cases}. \tag{13}$$

Once the vehicle body flexibility is considered in addition to the rigid body motions described in the last subsection, the bending modes are included. As shown in figure 3, the

Downloaded by [Kungliga Tekniska Hogskola] at 04:36 26 November 2015

Downloaded by [Kungliga Tekniska Hogskola] at 04:36 26 November 2015

flexible deformation of the vehicle body beam can be described by $\bar{x}(l,t)$, where l represents the distance along the beam and t the time [12, 29]. At the ith mode frequency of the beam, ω_i, the deformation can be expressed as

$$\bar{x}_i(l,t) = Z_i(l)\Phi_i(t) \tag{14}$$

where $\Phi_i(t)$ is a function of t alone and $Z_i(l)$ an eigenfunction, which describes the mode shape of the beam at ω_i. The elastic body has an infinite number of vibration modes; its dynamic response may be calculated as the sum of principal mode contributions. Since the system is linear, the total deformation of the vehicle body beam is the superposition of the principal modes, that is,

$$\bar{x}(l,t) = \sum_{i=1}^{\infty} Z_i(l)\Phi_i(t). \tag{15}$$

Using the orthogonal properties of principal modes, we can obtain the following equation

$$M_i\ddot{\Phi}_i(t) + \vartheta\gamma_i\dot{\Phi}_i(t) + \gamma_i\Phi_i(t) = f_A Z_i(b_1) + f_B Z_i(b_2) \tag{16}$$

where ϑ is a damping coefficient, M_i and γ_i are the modal mass and stiffness coefficients which can be further described as

$$\begin{cases} M_i = \int_0^L \rho A Z_i^2(l)dl \\ \gamma_i = M_i\omega_i^2 \end{cases} \tag{17}$$

where ρA is mass per unit length. In equation (16), f_A and f_B are suspension forces applied at points A and B, respectively. They can be formulated as

$$\begin{cases} f_A = -k_1(x_2 - x_1) - c_1(\dot{x}_2 - \dot{x}_1) + u_1 \\ f_B = -k_2(x_4 - x_3) - c_2(\dot{x}_4 - \dot{x}_3) + u_2 \end{cases} \tag{18}$$

where x_2 and x_4 are the total displacements including the contributions from both the rigid and flexible vehicle body modes. The total displacement of the vehicle body at a point, which is measured from the rear end to a distance l, can be formulated as

$$x(l,t) = x_5 + (l - a_2 - b_2)\varphi + \sum_{i=1}^{\infty} Z_i(l)\Phi_i(t). \tag{19}$$

In the following description, the first three bending modes of the flexible body beam are considered. Combining the rigid and flexible body motions, the model corresponding to the vehicle body will consider the two rigid body modes (pitch and heave modes) and the first three bending modes.

By combining the rigid half-vehicle model described in the previous subsection with the linear flexible vehicle body beam model, we can have the system state equation in matrix

form as

$$\dot{\mathbf{x}} = \mathbf{A}\mathbf{x} + \mathbf{B}\mathbf{u} + \mathbf{D}_1\mathbf{w} + \mathbf{D}_2\dot{\mathbf{w}} \tag{20}$$

where the state variables $\mathbf{x}$, actuator forces $\mathbf{u}$, and road excitations $\mathbf{w}$, are described as follows

$$\begin{cases} \mathbf{x} = [x_2 - x_1 \quad x_4 - x_3 \quad \dot{x}_5 \quad \dot{\varphi} \quad x_1 \quad \dot{x}_1 \quad x_3 \quad \dot{x}_3 \quad \Phi_1 \quad \dot{\Phi}_1 \quad \Phi_2 \quad \dot{\Phi}_2 \quad \Phi_3 \quad \dot{\Phi}_3]^T \\ \mathbf{u} = [u_1 \quad u_2]^T \\ \mathbf{w} = [w_1 \quad w_2]^T \end{cases} \tag{21}$$

and matrices $\mathbf{A}$, $\mathbf{B}$, $\mathbf{D}_1$ and $\mathbf{D}_2$ of dimensions 14×14, 14×2, 14×2 and 14×2, respectively, are offered in the Appendix. To compare the results from the current research with those by Hac [12], note that the state variables in equation (21) for the rigid body motions are different from those in equation (6).

If the augmented state vector $\mathbf{x}_a$ is as follows

$$\mathbf{x}_a = \begin{bmatrix} \mathbf{x}^{\mathbf{T}} & \mathbf{w}^{\mathbf{T}} \end{bmatrix}^T \tag{22}$$

then we can obtain the augmented state space equations in matrix form as

$$\begin{cases} \dot{\mathbf{x}}_a = \mathbf{A}_a\mathbf{x}_a + \mathbf{B}_a\mathbf{u} + \mathbf{D}_a\xi \\ \mathbf{y}_a = \mathbf{C}_a\mathbf{x}_a \end{cases} \tag{23}$$

where the matrices $\mathbf{A}_a$, $\mathbf{B}_a$, and $\mathbf{D}_a$ are defined as

$$\begin{cases} \mathbf{A}_a = \begin{bmatrix} \mathbf{A} & \mathbf{D}_1 + \mathbf{D}_2\mathbf{F}_w \\ \mathbf{0}_{2\times 14} & \mathbf{F}_w \end{bmatrix} \\ \mathbf{B}_a = \begin{bmatrix} \mathbf{B}^T & \mathbf{0}_{2\times 2} \end{bmatrix}^T \\ \mathbf{D}_a = \begin{bmatrix} \mathbf{D}_w^T\mathbf{D}_2^T & \mathbf{D}_w^T \end{bmatrix}^T \end{cases} \tag{24}$$

where both $\mathbf{F}_w$ and $\mathbf{D}_w$ are of dimension 2×2 and they can be obtained from equation (10).

Since the velocities of the front and rear unsprung masses and two points (the rear and front ends) or three points (the rear end, front end, and middle point) on the vehicle body are assumed to be measured, the output matrix $\mathbf{C}_a$ has the dimension of 4×16 or 5×16 accordingly. The corresponding output matrix is shown in the Appendix.

4. Algorithms and implementation of optimization problem

In this section, the LQG control [10, 12, 14, 26, 28, 30] and the Kalman filter [12, 26, 28] algorithms are recalled; then the optimization problem is described. In the development of the LQG controller and Kalman estimator, the 'separation principle' was adopted. First, the optimal controller is designed as if full state feedback is available; second, the optimal estimator is designed to provide the full state estimation.

Downloaded by [Kungliga Tekniska Hogskola] at 04:36 26 November 2015

4.1 *LQG control strategy*

The LQG control strategy can be described as an optimization problem: minimize the following objective function or performance index

$$J = \lim_{T\to\infty} \frac{1}{T} E\left\{ \int_0^T \begin{bmatrix} \mathbf{x}_a \\ \mathbf{u} \end{bmatrix}^T \begin{bmatrix} \mathbf{G} & \mathbf{N} \\ \mathbf{N}^T & \mathbf{H} \end{bmatrix} \begin{bmatrix} \mathbf{x}_a \\ \mathbf{u} \end{bmatrix} dt \right\} \tag{25}$$

subject to the first equation of (23). In equation (25), **G**, **N** and **H** are weighting matrices with proper dimensions.

The solution to the optimization problem is the control force vector with the following form:

$$\mathbf{u} = -\mathbf{K}\mathbf{x}_a \tag{26}$$

where the control gain matrix **K** is determined by

$$\mathbf{K} = \mathbf{H}^{-1}(\mathbf{N}^T + \mathbf{B}_a^T\mathbf{S}) \tag{27}$$

where the symmetric and positive-definite matrix **S** is a solution of the Riccati equation:

$$\mathbf{S}\mathbf{A}_a + \mathbf{A}_a^T\mathbf{S} + \mathbf{G} - (\mathbf{S}\mathbf{B}_a + \mathbf{N})\mathbf{H}^{-1}(\mathbf{S}\mathbf{B}_a + \mathbf{N})^T = \mathbf{0}. \tag{28}$$

The covariance matrix $\mathbf{X}_a$ of the state variable vector $\mathbf{x}_a$ is obtained from:

$$\mathbf{X}_a = E[\mathbf{x}_a\mathbf{x}_a^T] \tag{29}$$

where $\mathbf{X}_a$ is a function of the autocorrelation of vector ξ. For example, if there are only two road inputs, $\mathbf{X}_a$ is determined by the Lyapunov equation

$$(\mathbf{A}_a - \mathbf{B}_a\mathbf{K})\mathbf{X}_a + \mathbf{X}_a(\mathbf{A}_a - \mathbf{B}_a\mathbf{K})^T + \mathbf{Q}_1 = \mathbf{0} \tag{30}$$

where the matrix $\mathbf{Q}_1$ is determined by whether there is a time delay between the two inputs or not. The matrix $\mathbf{Q}_1$ [30] can be calculated by

$$\mathbf{Q}_1 = \begin{cases} \mathbf{D}_a\mathbf{Q}\mathbf{D}_a^T & \textit{without time delay} \\ \mathbf{D}_a\mathbf{Q}\mathbf{D}_a^T + Q_0(\mathbf{D}_{a2}\mathbf{D}_{a1}^T\boldsymbol{\Theta}^T(D) + \boldsymbol{\Theta}(D)\mathbf{D}_{a1}\mathbf{D}_{a2}^T) & \textit{with time delay} \end{cases} \tag{31}$$

where the matrix **Q**, the constant Q_0 and the time delay D are given by equations (13), (12) and (7), respectively, and $\boldsymbol{\Theta}(D)$ is the system transition matrix that is defined as

$$\boldsymbol{\Theta}(D) \triangleq \exp(\mathbf{A}_a \cdot D). \tag{32}$$

$\mathbf{D}_{a1}$ and $\mathbf{D}_{a2}$ are the two columns of $\mathbf{D}_a$, *i.e.*,

$$\mathbf{D}_a = \begin{bmatrix} \mathbf{D}_{a1} & \mathbf{D}_{a2} \end{bmatrix}. \tag{33}$$

The resulting performance index is expressed as

$$J_{opt} = trace(\mathbf{S}\mathbf{Q}_1). \tag{34}$$

Downloaded by [Kungliga Tekniska Hogskola] at 04:36 26 November 2015

Downloaded by [Kungliga Tekniska Hogskola] at 04:36 26 November 2015

4.2 *Kalman filter algorithm*

The LQG algorithm outlined above assumes perfect measurement of all the state variables. In practice, not all the state variables are available but only a limited number of the states [12, 26, 28]. In addition, the measurements are noisy.

It is assumed that the measurements are corrupted by noise. Thus, with equation (23), the measurement equation can be as follows:

$$\mathbf{y}_a = \mathbf{C}_a\mathbf{x}_a + \upsilon \tag{35}$$

where υ is assumed to be a Gaussian white noise process vector with zero mean and covariance matrix $\mathbf{R}$ described by

$$\begin{cases} E[\upsilon(t)] = \mathbf{0} \\ E[\upsilon(t)\upsilon(\tau)] = \mathbf{R}\delta(t-\tau) \end{cases} \tag{36}$$

where $\mathbf{R}$ is a positive definite matrix with proper dimensions.

Thus, the optimal estimator can be formulated as

$$\dot{\hat{\mathbf{x}}}_a = \mathbf{A}_a\hat{\mathbf{x}}_a + \mathbf{B}_a\mathbf{u} + \mathbf{L}(\mathbf{y}_a - \mathbf{C}_a\hat{\mathbf{x}}_a) \tag{37}$$

where $\hat{\mathbf{x}}_a$ is the optimal estimation of $\mathbf{x}_a$ and $\mathbf{L}$ the Kalman filter gain matrix that is determined by

$$\mathbf{L} = \mathbf{P}\mathbf{C}_a^T\mathbf{R}^{-1} \tag{38}$$

where $\mathbf{P}$ is the filter error ($\mathbf{e} = \hat{\mathbf{x}}_a - \mathbf{x}_a$) covariance matrix which can be found from the following steady-state matrix Riccati equation

$$\mathbf{A}_a\mathbf{P} + \mathbf{P}\mathbf{A}_a^T + \mathbf{Q}_1 - \mathbf{P}\mathbf{C}_a^T\mathbf{R}^{-1}\mathbf{C}_a\mathbf{P} = \mathbf{0}. \tag{39}$$

With the vehicle dynamic system described in equations (9) and (23), and the LQG controller and Kalman estimator designed previously, we can obtain the strongly coupled vehicle dynamic system, controller, and estimator as shown in figure 4 using a cascade arrangement.

Thus, the performance index of the assembled system is given by

$$J_{opt} = trace(\mathbf{S}\mathbf{Q}_1) + trace(\mathbf{K}^T\mathbf{H}\mathbf{K}\mathbf{P}). \tag{40}$$

The performance index consists of two parts. The first part denoted by J_Q results from the random road excitation while the second part denoted by J_r is due to the measurement errors.

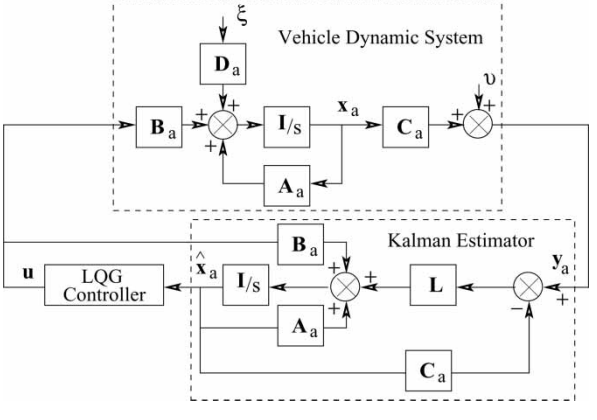

Figure 4. Cascade arrangement of vehicle dynamic system, Kalman estimator and LQG controller.

The presence of measurement error increases the performance index since $trace(\mathbf{K}^T\mathbf{HKP})$ is, in general, positive.

In addition to the performance measures, two other important aspects that can be used to evaluate active suspensions are the amount of control power and actuator force required. The average power delivered to a hydraulic or other type of actuator can be estimated by considering the forces and motions across that actuator. It is recommended [27] that the approximated average power is

$$P_{av} = u_p V_{av} \tag{41}$$

where u_p is the peak force produced by the actuator and V_{av} is the rectified average piston velocity. Suppose the force u_p and velocity V_{av} are individually Gaussian, which are linear combinations of the components of the state vector $\mathbf{x}$. Thus, the force and velocity can be obtained by

$$\begin{cases} u_p = 3\sqrt{E[(u)^2]} \\ V_{av} = \sqrt{2E[(V)^2]/\pi} \end{cases} . \tag{42}$$

Therefore, the average power can be determined by

$$P_{av} = 3\sqrt{2E[(u)^2] \cdot E[(V)^2]/\pi}. \tag{43}$$

4.3 *Formulation of the optimization problem*

Among the various MDO formulations, the A-i-O and Individual Discipline Feasible (IDF) methods are the two most common approaches [23]. The essence of the IDF is to maintain individual discipline feasibility, while allowing the optimizer to drive the individual disciplines to multidisciplinary feasibility and optimality by controlling the interdisciplinary coupling variables. In the IDF approach, some specific analysis variables representing communication, or coupling, between analysis disciplines via interdisciplinary mappings are 'promoted' to become optimization variables. These optimization variables are indistinguishable from design variables from the point of view of a single analysis discipline solver. In contrast with the A-i-O method, the relevant disciplines in an IDF approach are formulated in a parallel pattern with respect to the optimizer.

For the A-i-O and IDF methods, with moderate or no modification, they all have the advantage of using existing single discipline analysis codes. Compared with the A-i-O method, the IDF method may avoid the expensive procedure for achieving multidisciplinary feasibility at each optimization iteration. The computation efficiency of the IDF can be superior when the number of coupling variables and constraints is small.

As shown in figure 4, the vehicle dynamic system, controller and estimator are strongly coupled. If the IDF method is used for the vehicle system design optimization, in addition to the original design variable vector $\mathbf{X}_D$, the coupling variables, such as the control gain matrix $\mathbf{K}$ and the Kalman filter gain matrix $\mathbf{L}$, should be 'promoted' to become optimization variables. The large number of the 'promoted' design variables will result in expensive communication costs. Moreover, compared with the computer time used by A'GEM for generating the governing equations of the vehicle system or the time used by Kalman filter algorithm for optimizing the estimator, the time consumed by the LQG control algorithm for optimizing the controller is much longer. Note that the original design variable vector $\mathbf{X}_D$ may include the passive design variables for the vehicle system, e.g. inertial property parameters, geometric parameters and passive suspension parameters, and control parameters such as the weighting factors required in equation (25).

Downloaded by [Kungliga Tekniska Hogskola] at 04:36 26 November 2015

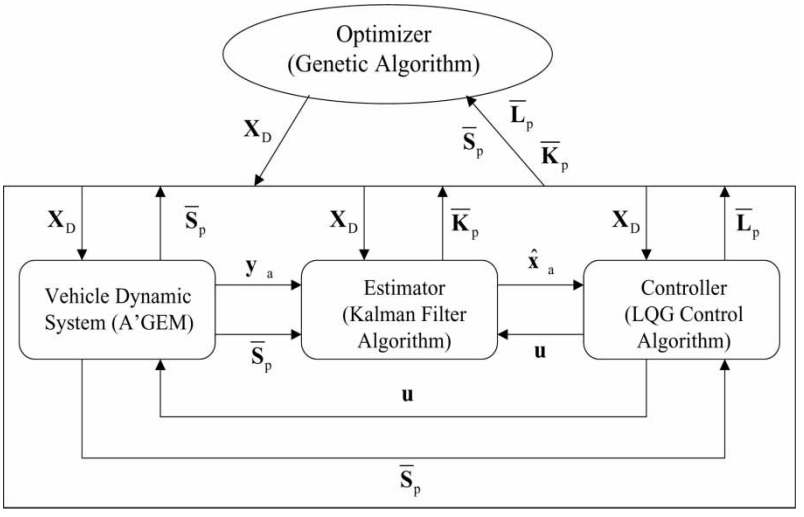

Figure 5. Schematic representation of the design optimization approach.

With the above considerations, the A-i-O method is applied to the vehicle system design for optimizing the mechanical subsystem, controller, and estimator simultaneously. Figure 5 shows the schematic representation of the design optimization approach.

The system shown in figure 5 is composed of an optimizer, i.e. a genetic algorithm that manipulates the relevant objective function and constraints, and three disciplines: the vehicle dynamic system with the A'GEM software, the optimal estimator with the Kalman filter algorithm and the optimal controller with the LQG control algorithm. The A-i-O approach to this optimization problem is a two-level optimization method. The optimization problem is solved for each discipline as well as for the system as a whole. The system is nonhierarchical because each discipline is coupled to every other discipline, and no discipline is viewed as being 'above' the others.

After a generation evolution of the GA, an individual design variable set $\mathbf{X}_D$ is provided by the GA to the coupled analysis disciplines. With this set of design variables, a complete system multidisciplinary analysis (MDA) is performed to obtain vehicle dynamic system output variable vector $\mathbf{y}_a$, optimal estimate vector $\hat{\mathbf{x}}_a$ and actuator force vector $\mathbf{u}$, which are used for evaluating the corresponding objective functions and constraints. In addition to these coupled variables among the three disciplines, the resulting vehicle system parameters $\bar{\mathbf{S}}_p$, *e.g.*, the system matrix $\mathbf{A}_a$ generated by the A'GEM software, are offered to the Kalman filter algorithm and the LQG control algorithm from the vehicle dynamic system for evaluating the above coupled variables. The vehicle system parameters $\bar{\mathbf{S}}_p$ together with the resulting Kalman estimator parameters $\bar{\mathbf{K}}_p$, such as the filter error covariance matrix $\mathbf{P}$, and the resulting LQG controller parameters $\bar{\mathbf{L}}_p$, such as the positive-definite matrix $\mathbf{S}$, are returned to the optimizer for the evaluation of the system objective function and constraints.

4.4 *Implementation of the optimization problem*

As shown in figure 6, the A-i-O method is implemented using a two-level optimization approach. At the system or discipline level, the GA is used to optimize the combined mechanical and control system, a synergistic whole. At the subsystem or subdiscipline level, the LQG and Kalman filter algorithms are utilized to optimize the controller and estimator, respectively.

Downloaded by [Kungliga Tekniska Hogskola] at 04:36 26 November 2015

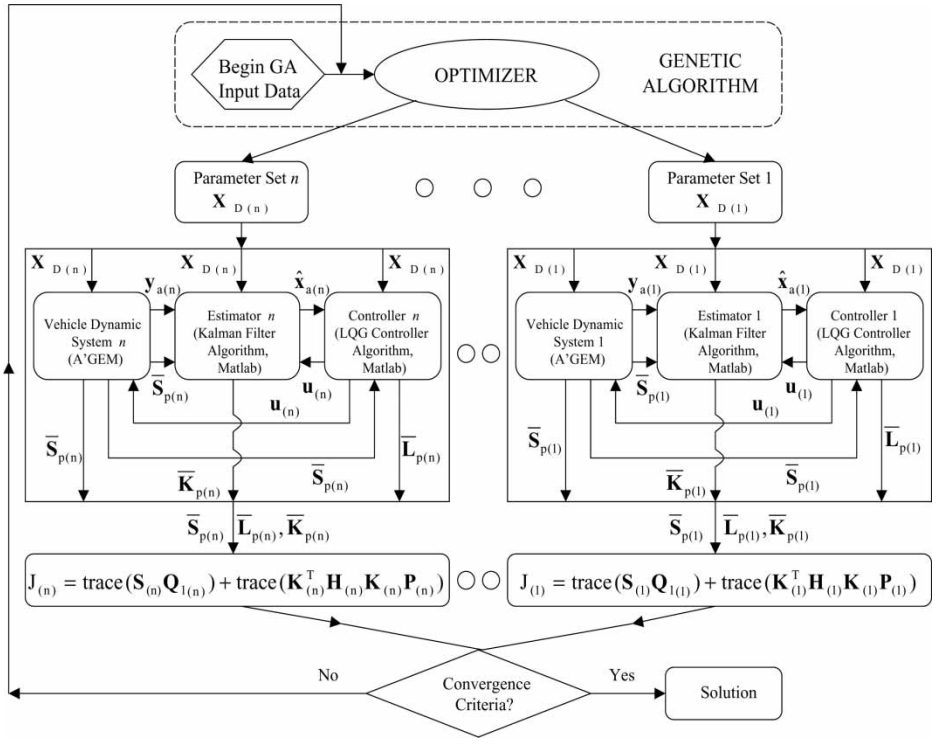

Figure 6. Schematic representation of the computer implementation for the A-i-O approach.

The GA is implemented using the MechaGen program that was developed by Baumal and McPhee at the University of Waterloo [6]. The MechaGen program is based on Goldberg's GA [34] and was written in C using pseudo-random number generators linked from the NAG (Numerical Algorithms Group) Fortran library. However, to avoid premature termination of the algorithm, instead of using a weighted roulette wheel based on the fitness sum of the population for the reproduction stage, one based on the ranking of the population according to fitness is used [35]. In addition, to improve the efficiency of the GA, the binary strings and fitness values for each unique design of the current generation are stored in a linear search look-up table. If a design string in the next generation matches one in the table, then the fitness does not have to be re-calculated. This saves significant computing time, given the computational expense of optimizing the vehicle system using the A-i-O formulation method.

With the implementation of the GA, a population of designs evolves from generation to generation through the application of the genetic operators, i.e. selection, crossover and mutation. Selection is a process in which individual strings are copied based on their fitness values. Highly fit strings (good designs) have a higher number of offspring in the succeeding generation. Crossover is a method of combining successful individuals by exchanging equivalent lengths of their chromosomes. Two strings from the reproduced population are mated randomly, and a crossover site is selected at random. Mutation is a technique that introduces new information into the new population at the bit level. A set of bits are selected randomly within the entire population. After performing selection, crossover and mutation, the GA generates a new population with potentially more individuals of higher fitness value. With enough repetitions of the cycle, the population will converge to the chromosome/design with the highest fitness.

Downloaded by [Kungliga Tekniska Hogskola] at 04:36 26 November 2015

Downloaded by [Kungliga Tekniska Hogskola] at 04:36 26 November 2015

With the aid of figure 4, figure 6 shows the multidisciplinary analysis and its feasibility requirement of the A-i-O optimization problem. As illustrated in figure 6, first, a population of n sets of design variables, $\mathbf{X}_{D(i)}$ (including inertial parameters $\mathbf{In}_i$, geometric parameters $\mathbf{G}_i$, and passive suspension parameters $\mathbf{S}_i$, where $i = 1, 2, \ldots, n$), are randomly selected in the search space by the GA; the corresponding set of design variables is sent in parallel to the coupled vehicle dynamic system with the A'GEM software, the estimator with the Kalman filter algorithm, and the controller with the LQG algorithm. Given the parameter set $\mathbf{X}_{D(i)}$, a complete multidisciplinary analysis (MDA) is performed: the A'GEM routines automatically generate the equations of motions in a state space form for vehicle dynamic system i; with the required vehicle dynamic system matrices and weighting factors, the LQG algorithm and the Kalman filter algorithm in MATLAB construct and optimize controller i and estimator i, respectively. This multidisciplinary analysis results in vehicle dynamic system output vector $\mathbf{y}_{a(i)}$, optimal estimator output vector $\hat{\mathbf{x}}_{a(i)}$ and actuator force vector $\mathbf{u}_{(i)}$, which are used for evaluating the corresponding performance indices and constraints. In addition to these coupled variables among the three disciplines, the resulting vehicle system parameters $\bar{\mathbf{S}}_{p(i)}$, such as the system matrix $\mathbf{A}_{a(i)}$ generated by the A'GEM software, are offered to the Kalman filter algorithm and the LQG control algorithm for evaluating the above coupled variables. The vehicle system parameters $\bar{\mathbf{S}}_{p(i)}$ together with the resulting Kalman estimator parameters $\bar{\mathbf{K}}_{p(i)}$ (e.g. the filter error covariance matrix $\mathbf{P}_{(i)}$), and the LQG controller parameters $\bar{\mathbf{L}}_{p(i)}$ (e.g. the positive-definite matrix $\mathbf{S}_{(i)}$) are returned for the evaluation of the system performance index $J_{(i)} = trace(\mathbf{S}_{(i)}\mathbf{Q}_{1(i)}) + trace(\mathbf{K}_{(i)}^T\mathbf{H}_{(i)}\mathbf{K}_{(i)}\mathbf{P}_{(i)})$. Then these performance indices (i.e. $\{J_{(1)}, J_{(2)}, \ldots, J_{(n)}\}$), are used as the fitness values. At this point, if the convergence criteria are satisfied, the calculation terminates; otherwise these fitness values are returned to the GA. Based on the returned fitness values corresponding to the given sets of design variables, the GA produces the next generation of design variable sets using the genetic operators, reproduction, crossover and mutation. This procedure repeats until the optimized variable set is found.

Note that the above implementation of the A-i-O approach is based on the random road input case. In the deterministic road input case, the implementation is modified accordingly.

In the study, all computations were carried out on a Silicon Graphics Indigo 2 XZ workstation. The GA (MechaGen program written in C), A'GEM package (written in Fortran) and MATLAB (version 5.2) were linked by a main Fortran program and implemented on the workstation. In the numerical experiments of the A-i-O method shown in figure 6, it was found by trial and error that consistent results were obtained for the GA using a crossover probability of 100%, a mutation probability of 1.0% and a population size (the number of design variable sets) of 120.

In the random input case, to optimize the passive vehicle system variables (shown later in table 8), the LQG control gain matrix $\mathbf{K}$, and the Kalman filter gain matrix $\mathbf{L}$, the elapsed time of operating the A-i-O method took 12.53 h for 6936 fitness evaluations. In the deterministic road input case, the operation of the A-i-O method required 13.27 h for 7125 fitness evaluations.

It was found that the data communication among the A'GEM program, the LQG control routines and the Kalman filter routines and opening the MATLAB engine (once per multidisciplinary analysis) from the main Fortran program occupied a large portion of the elapsed time. Therefore, if the routines for the LQG control algorithm and the Kalman filter algorithm are coded in Fortran or C and combined with the main Fortran program (instead of running these routines in MATLAB), the A-i-O method will be much more efficiently implemented. Moreover, the numerical multibody dynamics package A'GEM generates the equations of motion of the vehicle system for each GA population member at each generation in the implementation of the A-i-O method. If a symbolic multibody dynamics program is used for this purpose, it will generate the equations of motion once in a symbolic format. By substituting individual design variable set $\mathbf{X}_{D(i)}$ into the symbolic equations, the required equations for the

multidisciplinary analysis can be obtained. This will improve the efficiency for implementing the A-i-O method. With the parallelism property of the GA, the A-i-O method is suitable for applications using massively parallel computers. If the current applications are implemented in a massively parallel computer system, the computation time could be reduced approximately by a factor of the population size of the GA [35].

5. Numerical simulations

In this section, the simulation results for the half-vehicle models with rigid and flexible vehicle bodies are provided and analysed. For the rigid body vehicle model, the simulations are carried out with the road inputs selected as unit step inputs corresponding to the integrated white noise road input case. For the flexible body vehicle model, the numerical optimization is performed under the condition that the road inputs are the filtered white noise processes. For both the vehicle models, it is supposed that the road disturbance inputs at the front and rear unsprung masses are identical except that the latter is delayed by the time interval D with respect to the former. The numerical results based on the A-i-O method are compared with those based on the LQG algorithm and the corresponding passive suspensions.

Note that the objective of this section is to demonstrate the feasibility and efficacy of the design methodology introduced in section 2. In the application of this methodology to the optimization of the half-vehicle models with active suspensions, some interesting results were obtained. Thus, in this section, these results are also discussed and investigated.

5.1 *Rigid vehicle body with deterministic road input case*

5.1.1 Vehicle system optimization. The vehicle system optimization problem is to minimize the following objective function:

$$J = \int_0^\infty [\rho_1 \ddot{x}_2^2 + \rho_2 \ddot{x}_4^2 + \rho_3 (x_1 - w_1)^2 + \rho_4 (x_3 - w_2)^2 + \rho_5 (x_2 - x_1)^2 + \rho_6 (x_4 - x_3)^2]\, dt \tag{44}$$

or

$$J = \sum_{i=1}^{6} \rho_i J_i \tag{45}$$

subject to

$$\dot{\mathbf{x}} = \mathbf{A}\mathbf{x} + \mathbf{B}\mathbf{u} + \mathbf{D}\dot{\mathbf{w}} \tag{46}$$

where the vectors **x**, **u**, and **w** are defined by equation (6) and the system, control and disturbance matrices (**A**, **B**, and **D**) are provided in the Appendix. The design variables include the LQG control gain matrix **K** and passive vehicle system parameters, i.e. inertial parameters, geometric parameters, and suspension parameters as shown in table 3. In the objective function shown in (45), ρ_1 to ρ_6 are the weighting factors, J_1 to J_6 are defined in table 1, and $\rho_1 J_1$ to $\rho_6 J_6$ imply the measurements of the vertical accelerations of the vehicle body at points A and B (see figure 3), the unsprung mass dynamic loads of m_1 and m_2, and front and rear secondary suspension working spaces, respectively. The governing equations of the vehicle system show that $\ddot{x}_2$ and $\ddot{x}_4$ are dependent on the front and rear secondary suspension forces, respectively. Hence, constraining the accelerations at points A and B of the vehicle body also constrains

Downloaded by [Kungliga Tekniska Hogskola] at 04:36 26 November 2015

Table 1. Expressions represented by symbols J_1 to J_6.

$J_1 = \int_0^\infty \ddot{x}_2^2 dt$	$J_2 = \int_0^\infty \ddot{x}_4^2 dt$	$J_3 = \int_0^\infty (x_1 - w_1)^2 dt$
$J_4 = \int_0^\infty (x_3 - w_2)^2 dt$	$J_5 = \int_0^\infty (x_2 - x_1)^2 dt$	$J_6 = \int_0^\infty (x_4 - x_3)^2 dt$

the actuator forces u_1 and u_2 and front and rear passive secondary suspension forces. Note that the constraint shown in equation (46) is satisfied when the corresponding multidisciplinary feasibility requirement is met during the implementation of the A-i-O approach.

To facilitate the optimization and the control law synthesis, each term of the objective function shown in equation (44) is normalized with the corresponding norm. The norm of each term is the inverse of the corresponding weighting factor. The weighting factors are assumed to be

$$\rho_i = 1/J_i^{ref} \tag{47}$$

where $i = 1, 2, \ldots, 6$, and J_i^{ref} is the ith term of the objective function (in the form of equation (45)) of a reference half-vehicle model with passive or active suspensions. Note that the definition of J_i^{ref} $(i = 1, 2, \ldots, 6)$ is the same as its counterpart (J_i) shown in table 1.

The objective function, as provided by equation (44), quadratically penalizes large deviations of the state and control vectors from their desired set point values. Numerical experiments show that the selection of the weighting factors for the objective function is important and greatly affects the implementation of the A-i-O method. With each penalized variable normalized by the mean-square value of the corresponding variable of a reference vehicle model (see equation (47)), each term of the objective function can be guaranteed to be at the same order of digital value during the optimization and the GA can effectively coordinate the design criteria of ride comfort, suspension working space, dynamic wheel load and actuator force. Form the designer's point of view, this is a meaningful form of objective function because it requires that only an appropriate reference vehicle model be selected.

Note that to find the solution to the optimization problem, equation (44) should be formulated in the standard matrix form as shown in equation (25).

5.1.2 Results and discussion. In this subsection, the simulation results from the A-i-O method are discussed and compared with those reported by Thompson [10]. As will be seen, the optimized vehicle model based on the A-i-O method has better performance than the corresponding model with passive suspension and that based on the LQG algorithm (used by Thompson) in all four aspects: ride comfort, suspension working spaces, unsprung mass dynamic loads and actuator forces. Note that the simulation results reported by Thompson [10] have been accurately repeated in this research. Moreover, in the simulation, the step input of road position is set as 0.01 m.

Based on the half-vehicle model with active suspension designed by Thompson [10], the weighting factors ρ_1, ρ_2, ρ_3, ρ_4, ρ_5, and ρ_6 are assigned the values of 5.4190×10^{-4}, 2.2261×10^{-4}, 78.8781, 50.7307, 13.7052 and 14.6588, respectively. Using the A-i-O method, we can find the control gain matrix **K** listed in table 2 together with that based on Thompson's method (the LQG algorithm). In the A-i-O case, the additional design variables are selected as m_1, m_2, M, I_c, a, b, k_1, c_1, k_2, c_2, k_3 and k_4. The design variables k_1, c_1, k_2 and c_2 are permitted to vary by 50% from their nominal values and the rest to vary by 10% from the nominal values. The corresponding optimal values for these design variables are provided in table 3.

In the A-i-O, LQG, and passive suspension cases, the selected resulting vehicle dynamic responses in the time domain are illustrated in figures 7, 8 and 9. In both the LQG and passive

Downloaded by [Kungliga Tekniska Hogskola] at 04:36 26 November 2015

Table 2. Feedback control gain matrix for optimal suspensions.

A-i-O							
$K_{1,1}$	$K_{1,2}$	$K_{1,3}$	$K_{1,4}$	$K_{1,5}$	$K_{1,6}$	$K_{1,7}$	$K_{1,8}$
−51636.0	30492.0	−315.0	352.0	61.0	4506.0	−8.0	38.0
$K_{2,1}$	$K_{2,2}$	$K_{2,3}$	$K_{2,4}$	$K_{2,5}$	$K_{2,6}$	$K_{2,7}$	$K_{2,8}$
−1111.0	381.0	−61896.0	48182.0	−12.0	52.0	553.0	3239.0
LQG							
$K_{1,1}$	$K_{1,2}$	$K_{1,3}$	$K_{1,4}$	$K_{1,5}$	$K_{1,6}$	$K_{1,7}$	$K_{1,8}$
−58092.0	35355.0	1392.0	−75.0	−1379.0	4620.0	−18.0	215.0
$K_{2,1}$	$K_{2,2}$	$K_{2,3}$	$K_{2,4}$	$K_{2,5}$	$K_{2,6}$	$K_{2,7}$	$K_{2,8}$
1058.0	75.0	−68826.0	35355.0	−8.0	233.0	−1774.0	4047.0

Downloaded by [Kungliga Tekniska Hogskola] at 04:36 26 November 2015

suspension cases, the parameters listed in table 3 take the nominal values. Figures 7, 8 and 9 demonstrate the relationships of vertical accelerations of the vehicle body at points A and B versus time and the pitch angular acceleration of the vehicle body versus time, respectively. Based on figures 7 and 8, we find that, among the three cases, the active suspension based on the A-i-O is best controlled with the smallest overshoots in accelerations of the vehicle body at both points A and B and the passive suspension behaves the worst with the largest overshoots. A close observation of figure 7 discloses that at the time the unit step input imposes on the unsprung mass m_2, this road disturbance affects the acceleration of the vehicle body at point A for all of the three cases. The disturbance is reflected by the rise in the second peak around the time on the corresponding acceleration curve for each case. In both the LQG and passive suspension cases, the time delay between the front and rear inputs is about 0.086 s. In the A-i-O case, the time delay is about 0.077 s. Compared with the acceleration of the vehicle body at point A, the road input at m_2 has a much more significant effect on the acceleration at point B. This difference can be found by the comparison of the second peak on each acceleration curve in figure 7 with the corresponding first peak in figure 8 for all of the three cases. Moreover,

Table 3. Optimized values for passive vehicle system design variables.

NV†					
m_1 (kg)	m_2 (kg)	M (kg)	I_c (kg m^2)	a_1 (m)	a_2 (m)
28.58	54.43	505.1	651.0	1.0978	1.4676
k_1 (N/m)	c_1 (N/m/s)	k_2 (N/m)	c_2 (N/m/s)	k_3 (N/m)	k_4 (N/m)
19960.0	2014.0	22590.0	2082.0	155900.0	155900.0
A-i-O					
m_1 (kg)	m_2 (kg)	M (kg)	I_c (kg m^2)	a_1 (m)	a_2 (m)
25.72	48.99	555.5	715.9	0.9880	1.3215
k_1 (N/m)	c_1 (N/m/s)	k_2 (N/m)	c_2 (N/m/s)	k_3 (N/m)	k_4 (N/m)
19777.2	1540.1	12365.2	2316.6	140802.9	170755.4

†Nominal values.

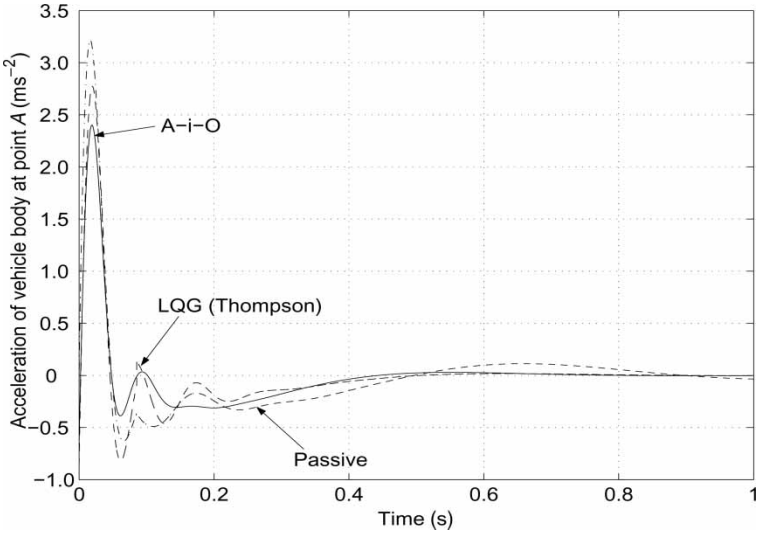

Figure 7. Acceleration of vehicle body at point A versus time.

as we can see from figure 8, in the case of LQG, the acceleration of the vehicle body at point B trembles immediately after the unit step input is imposed on the unsprung mass m_2. In the aspect of the angular acceleration of the vehicle body, as shown in figure 9, the active suspension based on the A-i-O method outruns those based on the LQG algorithm and the passive suspension with less magnitude.

Numerical experiments also show that, among the A-i-O, LQG, and passive suspension cases, the active suspension based on the A-i-O method is best controlled with smallest overshoot in both m_1 and m_2 displacements but the one based on the LQG has the largest overshoot. Results also reveal that, compared with the active suspension based on the LQG, the one based on the A-i-O behaves better with less overshoot in both front and rear secondary suspension

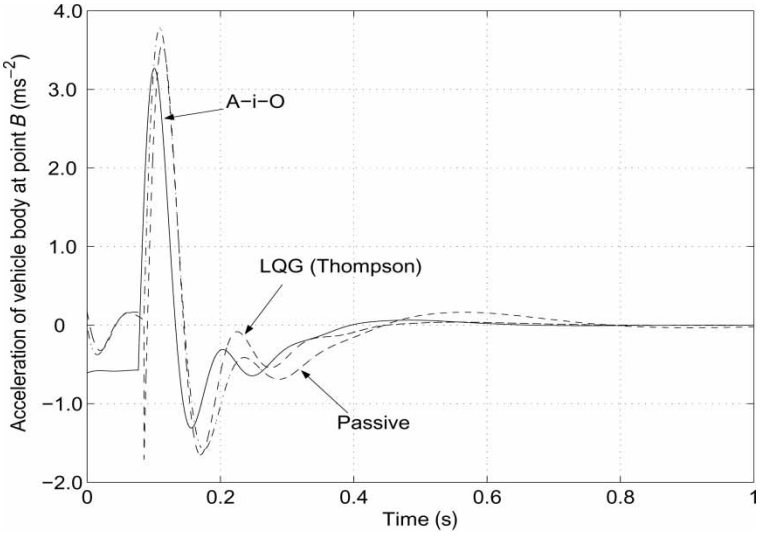

Figure 8. Acceleration of vehicle body at point B versus time.

Downloaded by [Kungliga Tekniska Hogskola] at 04:36 26 November 2015

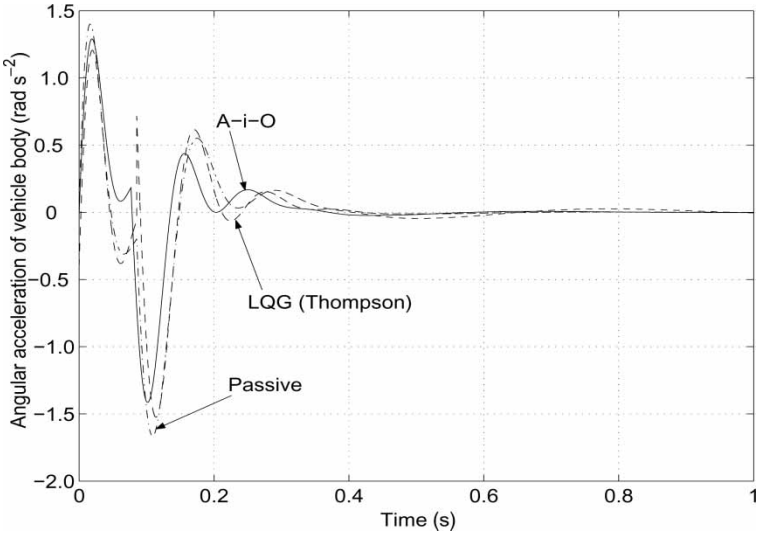

Figure 9. Pitch angular acceleration of vehicle body versus time.

working spaces. Although the passive suspension has less front and rear secondary suspension working space overshoot than the active suspensions, the oscillation is damped out much slower than those in the active suspensions.

Figures 10 and 11 illustrate the relationship between the corresponding secondary suspension force and time for both the front and rear secondary suspensions. Note that in figures 10 and 11, the total secondary suspension force based on the A-i-O consists of two sections: the active force (actuator force, denoted as A-i-O (active)) and the passive force (summation of passive spring and damper forces, denoted as A-i-O (passive)). A close observation of figure 10 reveals that, at a point when the road unit input imposes on the unsprung mass m_1,

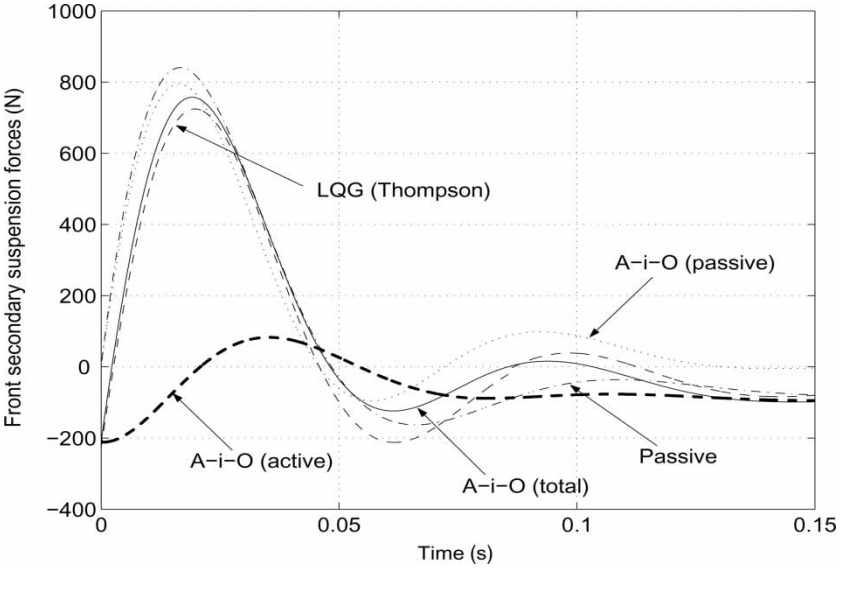

Figure 10. Front secondary suspension forces versus time.

Downloaded by [Kungliga Tekniska Hogskola] at 04:36 26 November 2015

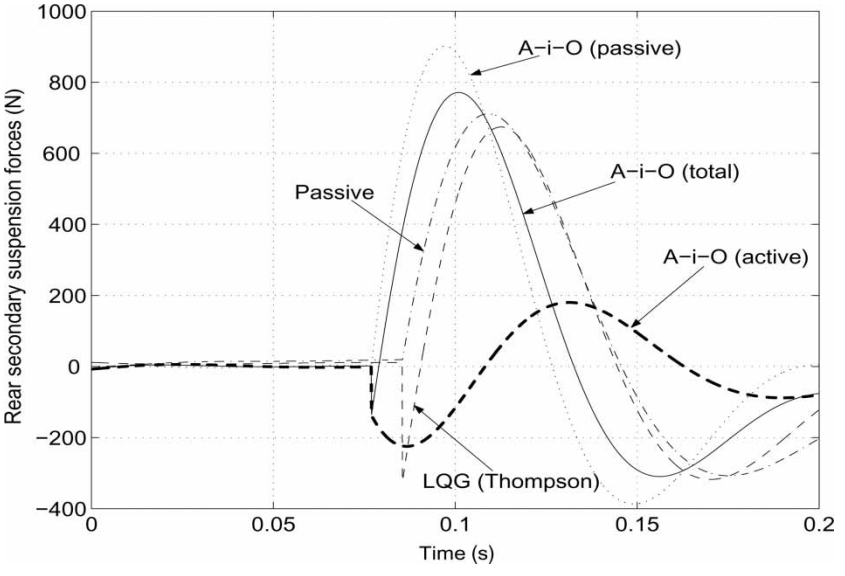

Figure 11. Rear secondary suspension forces versus time.

the corresponding active suspension force actively resists the disturbance immediately, but the corresponding passive suspension force just follows the disturbance. The resistance to the road disturbance contributes to the performance improvement of the corresponding suspension. Compared with the case of LQG, in the case of A-i-O, the active force resistance to the road disturbance lasts longer and the active force and the corresponding passive force are almost out of phase. This outphase between the active and passive forces in the case of A-i-O makes the corresponding total force smaller than the active force based on the LQG and leads to the performance improvement over the active suspension based on the LQG algorithm. In the case of LQG, although the active force resists the road disturbance, this resistance lasts a very short period of time. Then the active force follows the trends of the passive suspension force based on the A-i-O. Thus, the actuator force based on the A-i-O and that based on the LQG are also almost out of phase.

Interestingly, very similar curves as shown in figure 10 were also found in the analysis of a 2 DOF quarter-vehicle model with active suspension [14]. This similarity is due to the fact that the relevant vehicle system parameters for the quarter-vehicle model are the same as those in the front part of the half-vehicle model, e.g. the unsprung mass and the primary suspension spring stiffness coefficient. This similarity also supports the correctness of the calculation for the half-vehicle model.

A detailed comparison of figure 10 with 11 also reveals that after the point where the unit step input is imposed on the unsprung mass m_2, the trend of each curve in figure 11 is very similar to that of its counterpart in figure 10. Therefore, the previous force analysis for the front secondary suspension is also true for the rear secondary suspension of the half-vehicle model.

Note that the above optimal solution based on the A-i-O method is derived under the assumption that the actuators are capable of producing the optimized forces ideally. As mentioned in the introduction section, the optimal solution of actuator forces can be used as a desired design. In the refined design of an active suspension system (e.g. an electro-hydraulic suspension), the nonlinear dynamics of the electro-hydraulic actuators, the uncertainty of hydraulic

Downloaded by [Kungliga Tekniska Hogskola] at 04:36 26 November 2015

Table 4. Comparison of the response characteristics for passive and active suspensions.

	LQG	Passive	A-i-O
m_1 displacement overshoot (%)	28.80	17.05	16.57
m_2 displacement overshoot (%)	37.26	32.79	30.34
Peak front suspension working space (cm)	−1.16	−0.95	−1.06
Peak rear suspension working space (cm)	−1.17	−0.97	−1.06
Peak acceleration at point A (m/s^2)	2.77	3.22	2.40
Peak acceleration at point B (m/s^2)	3.57	3.78	3.27
Peak pitch acceleration (rad/s^2)	−1.52	−1.66	−1.42
Peak front actuator force (N)	724.6	0.0	−211.6
Peak rear actuator force (N)	674.1	0.0	−224.7
Peak passive front suspension force (N)	0.0	840.8	795.4
Peak passive rear suspension force (N)	0.0	711.2	901.9
Peak total front suspension force (N)	724.6	840.8	757.6
Peak total rear suspension force (N)	674.1	711.2	771.2
$\int_0^\infty 10^6(x_1 - w_1)^2 dt$ $(10^6 J_3)$	1.34	1.44	1.29
$\int_0^\infty 10^6(x_3 - w_2)^2 dt$ $(10^6 J_4)$	1.97	2.21	1.76
$\int_0^\infty 10^6(x_2 - x_1)^2 dt$ $(10^6 J_5)$	7.30	7.28	6.79
$\int_0^\infty 10^6(x_4 - x_3)^2 dt$ $(10^6 J_6)$	6.82	6.95	5.34
$\int_0^\infty 10\ddot{x}_2^2 dt$ $(10 J_1)$	1.85	2.68	1.39
$\int_0^\infty 10\ddot{x}_4^2 dt$ $(10 J_2)$	4.49	5.71	3.85
$\int_0^\infty 10\ddot{\varphi}^2 dt$	1.09	1.43	1.01
$\int_0^\infty 10^{-4} u_1^2 dt$	1.2595	0.0	0.1902
$\int_0^\infty 10^{-4} u_2^2 dt$	1.6164	0.0	0.2285
$\int_0^\infty 10^{-4} f_{1pass}^2 dt^\dagger$	0.0	1.8376	1.3538
$\int_0^\infty 10^{-4} f_{2pass}^2 dt^\ddagger$	0.0	2.0584	2.4395
$\int_0^\infty 10^{-4}(u_1 + f_{1pass})^2 dt$	1.2595	1.8376	1.3867
$\int_0^\infty 10^{-4}(u_2 + f_{2pass})^2 dt$	1.6164	2.0584	1.9992

$^\dagger f_{1pass}$ means passive front secondary suspension force.
$^\ddagger f_{2pass}$ means passive rear secondary suspension force.

parameters, and the bandwidth limitations of the system should be considered and alternative control algorithms may be used [24, 25].

To quantitatively analyse the vehicle performance based on the A-i-O, LQG, and passive suspension, the results are provided in table 4. The numerical results reveal that the active suspension based on the A-i-O method exhibits superior performance than its counterpart based on the LQG algorithm and the passive suspension in the mean-squared values of front and rear actuator forces, front and rear unsprung mass deflections, front and rear secondary suspension working spaces, accelerations of vehicle body at points A and B and pitch angular acceleration of vehicle body. In short, the active suspension based on the A-i-O method has the best overall performance among the three cases.

5.2 *Flexible vehicle body with random road input case*

In the analytical design of active vehicle suspensions, researchers usually use lumped vehicle models [31]. This approach is justified for compact vehicles like cars. However, for vehicles with a long wheelbase like rail vehicles and truck-trailers, because of the large deflections of the vehicle body, researchers often introduce an elastic element into the vehicle model [32]. Thus, in our application, the half-vehicle model with vehicle body flexibility is taken into account.

Downloaded by [Kungliga Tekniska Hogskola] at 04:36 26 November 2015

5.2.1 Vehicle system optimization. The vehicle system optimization can be stated as: minimize the objective function:

$$J = \sum_{i=1}^{4} \rho_i J_i \tag{48}$$

subject to the first equation of (23), where ρ_1 to ρ_4 are weighting factors and J_1 to J_4 are defined in table 5. J_2 is the mean squared acceleration at three or two body points denoted by l_1, l_2, and l_3 or by l_1 and l_2, which correspond to the rear end, front end and middle point of the vehicle body or the rear end and front end of the vehicle body, respectively. Due to the fact that the pitch mode and the first three bending modes of the elastic vehicle body are taken into account, the consideration of the acceleration at just one point is not justified. J_1, J_3 and J_4 are mean squared values of actuator forces, primary and secondary suspension deflections, respectively. To utilize the weighting constants used in the quarter-vehicle model reported in reference [11, 14] and compare our results with those offered by Hac [12], factors of $1/2$ and $1/3$ are introduced for the definitions described in table 5. The vehicle system, therefore, is optimized with respect to ride quality, unsprung mass dynamic loads and secondary suspension working spaces while the expenditure of actuator forces is limited.

As mentioned previously, to find the solution to the optimization problem, equation (48) should be rewritten in the standard matrix format as shown in (25).

5.2.2 Validation of the simulation results. Using the LQG algorithm, the vehicle model (half-vehicle model with flexible vehicle body), and the system parameters provided by Hac [12] (listed in table A2), numerical simulations were performed. Note that in the optimization of the controller for the active suspension of the half-vehicle model with flexible vehicle body, the objective function used by Hac [12] has a similar form as the one he used for the active suspension of the quarter-vehicle model [11]. Moreover, the control algorithm used by Hac for the half-vehicle model is mainly based on the one he used for the quarter-vehicle model. In the case of the quarter-vehicle model, the simulation results reported by Hac have been accurately repeated in our research. However, in the case of the half-vehicle model with flexible vehicle body, the simulation results reported by Hac could not be repeated. Compared with the quarter-vehicle model case, since the flexibility of the vehicle body is considered, the objective function in the half-vehicle model case is much more complicated. Expressed in terms of state and control variables and expanded in Maple [33] symbolic form, the objective function for the flexible vehicle model in equation (48) covers 372 pages (A4 paper). The complex and lengthy objective function seems to be the reason why Hac's numerical results do not agree with those from our research. Thus, the validation of our simulation results becomes necessary.

To validate our simulation results, the results based on a decoupled half-vehicle model are compared to those derived from the equivalent quarter-vehicle model developed by Hac [11].

To facilitate the validation, the decoupled half-vehicle model is constructed: the vehicle body is assumed to be rigid and parameters b_2 and I_c are set to 0.0 m and 1.6×10^5 kg m^2,

Table 5. Expressions represented by symbols J_1 to J_4.

$J_1 = E[u_1^2 + u_2^2]/2$
$J_2 = E\{\sum_{i=1}^{3 \text{ or } 2}[\ddot{x}_5 + (L_i - a_2 - b_2)\ddot{\varphi} + \sum_{j=1}^{3} \ddot{\Phi}_j(t) Z_j(L_i)]^2\}/3$
$J_3 = E\{[x_1 - w(t-D)]^2 + [x_3 - w(t)]^2\}/2$ †
$J_4 = E[(x_2 - x_1)^2 + (x_4 - x_3)^2]/2$

† $w(t-D) = w_1;\ w(t) = w_2$.

Downloaded by [Kungliga Tekniska Hogskola] at 04:36 26 November 2015

Downloaded by [Kungliga Tekniska Hogskola] at 04:36 26 November 2015

respectively, so that the front and rear suspensions of the model are inertially decoupled; the rest of the system parameters take their nominal values (listed in table A2). Furthermore, it is assumed that the time delay between the front and rear road inputs is neglected. Thus, the decoupled model is theoretically equivalent to two identical independent quarter-vehicle models. For the equivalent quarter-vehicle models, the sprung mass takes the value of 5000.0 kg and the remaining system parameters take the values of those of the decoupled half-vehicle model.

The objective function for the decoupled half-vehicle model is the same as that described in (48) except that the terms relevant to the bending modes of the flexible vehicle body are set to zero and J_2 is defined as $E[\ddot{x}_2^2 + \ddot{x}_4^2]/2$. The objective function of the equivalent quarter-vehicle model is the same as that used by Hac [11].

It is supposed that the velocity of both the decoupled half-vehicle model and the corresponding quarter-vehicle model $V = 20.0\,\mathrm{m/s}$ and the coefficients in formula (8) describing road irregularities $a_t = 0.45\,\mathrm{m}^{-1}$ and $\sigma_t = 3.0 \times 10^{-4}\,\mathrm{m}^2$. For both the decoupled half-vehicle model and the equivalent quarter-vehicle model, with the weighting factors $\rho_2 = 1$, $\rho_3 = 10^5$, and $\rho_4 = 10^4$, based on the LQG algorithm, we obtain the results illustrated in table 6.

The comparison of the simulation results shown in table 6 demonstrates that the simulation results for the decoupled half-vehicle model accurately matches those for the equivalent quarter-vehicle model. Therefore, at least the rigid body half-vehicle model and the corresponding objective function are validated. This validated rigid body half-vehicle model and objective function can be used to serve as a reference to check the simulation results of the corresponding half-vehicle model with flexible vehicle body.

To check the simulation results of the half-vehicle model with flexible vehicle body with those based on the validated rigid body half-vehicle model, it is assumed that: for both vehicle models, the vehicle system parameters are set to their nominal values listed in table A2; the objective function takes the form described in equation (48); the random road characteristic parameters, vehicle speed and the weighting factors ρ_2, ρ_3, ρ_4 take the values offered above; the time delay between the random road input imposed on the front unsprung mass and that on the rear unsprung mass is neglected. Based on the LQG algorithm, we obtain the simulation results offered in table 7.

A comparison of the results offered in table 7 shows that the simulation results based on the flexible vehicle model are consistent with those based on the rigid vehicle model. The average performance index J of the flexible vehicle model is about 3.4% higher than that of the rigid vehicle model. This difference results from the fact that the first three bending modes of the

Table 6. Comparison of the simulation results for the decoupled half-vehicle model and the equivalent quarter-vehicle model.

ρ_1	$J/10^6$	J_1 (N^2)	$J_2/10^6$ (mm^2/s^4)	$J_3/10$ (mm^2)	$J_4/10^2$ (mm^2)
Equivalent quarter-vehicle model					
10^6	22.67194237	$6.11420577 \times 10^{-7}$	4.44329323	14.1729511	4.05569743
10^2	22.66585547	60.60964055	4.44333608	14.1701350	4.04632342
10^0	22.23322899	3.25419349×10^5	4.49419024	13.9139521	3.49966726
10^{-2}	20.16447360	2.03248582×10^7	6.11463790	11.4086591	2.43792797
10^{-4}	19.93633651	2.62068886×10^7	6.44708294	11.0998273	2.38680554
Decoupled half-vehicle model					
10^6	22.67194237	$6.11420576 \times 10^{-7}$	4.44329323	14.1729511	4.05569743
10^2	22.66585547	60.60964053	4.44333608	14.1701350	4.04632342
10^0	22.23322899	3.25419349×10^5	4.49419024	13.9139521	3.49966726
10^{-2}	20.16447360	2.03248583×10^7	6.11463791	11.4086591	2.43792797
10^{-4}	19.93633651	2.62068886×10^7	6.44708294	11.0998273	2.38680554

Table 7. Comparison of the simulation results for the rigid half-vehicle model and the flexible half-vehicle model.

ρ_1	$J/10^6$	J_1 (N^2)	$J_2/10^6$ (mm^2/s^4)	$J_3/10$ (mm^2)	$J_4/10^2$ (mm^2)
Flexible half-vehicle model					
10^6	27.0252	5.3235×10^{-7}	8.8036	14.3577	3.8638
10^2	27.0199	52.7369	8.8018	14.3570	3.8558
10^0	26.6553	2.6311×10^5	8.7125	14.2882	3.3915
10^{-2}	25.4346	7.9631×10^6	9.2387	13.4871	2.6290
10^{-4}	25.3494	9.2990×10^6	9.3393	13.4105	2.5987
Rigid half-vehicle model					
10^6	26.3059	5.5123×10^{-7}	8.1317	14.2957	3.8785
10^2	26.3004	54.6229	8.1298	14.2947	3.8704
10^0	25.9181	2.8002×10^5	8.0441	14.1904	3.4036
10^{-2}	24.4349	1.2310×10^7	8.7743	12.9029	2.6347
10^{-4}	24.2985	1.5485×10^7	8.9541	12.7367	2.6062
Rigid half-vehicle model with time delay					
10^6	26.2340	5.3767×10^{-7}	8.3051	14.2878	3.7129
10^2	26.2277	53.2799	8.3031	14.2865	3.7055
10^0	25.7958	2.7273×10^5	8.2043	14.1648	3.2763
10^{-2}	24.2993	1.2204×10^7	8.8644	12.8224	2.6261
10^{-4}	24.1704	1.5376×10^7	9.0365	12.6568	2.6036

Downloaded by [Kungliga Tekniska Hogskola] at 04:36 26 November 2015

flexible vehicle body degrade the overall performance of the vehicle. This overall performance degradation of the flexible vehicle model also reflects on the higher partial performance indices of the acceleration and unsprung mass displacement of the model as compared to those of the rigid vehicle model.

To investigate the effect of the time delay on the performance of the vehicle models, the simulation results with time delay for the rigid half-vehicle model are also provided in table 7. The simulation results show that with the time delay considered the overall performance improves. The results also demonstrate that 'the time delay available between the front and rear inputs appears to provide, in principle, an excellent opportunity to improve the rear axle actuator control' [26]. However, under the given simulation conditions, the degree of improvement is not high. Numerical experiments show that if the weighting factors $\rho_1 = 10^{-8}$, $\rho_2 = 1.0$, $\rho_3 = 10^4$ and $\rho_1 = 10^3$, the performance index J with time delay is 6.222% lower than that without time delay.

It should be mentioned that with the time delay considered, using the LQG algorithm, we should calculate the required transition matrix. In the case of the rigid half-vehicle model, the calculation of the transition matrix in Matlab does not converge until the 60th term of the series is reached. In the case of the flexible half-vehicle model, the calculation of the corresponding transition matrix does not converge even when the 80th term of the series is reached. When the calculation is carried out until the 100th term of the series, the result overflows. The Matlab simulation results show that some entries of the overflowed transition matrix take the value 'INF' and most of the entries take the value 'NaN'. Note that in Matlab 'INF' means positive infinity and 'NaN' undefined mathematical operations like $\infty - \infty$.

Therefore, it seems that it is not practical to calculate the transition matrix for a complicated vehicle dynamic model when the time delay is considered. To circumvent the calculation of transition matrix, the Pade approximation method is recommended [26], but additional state variables should be introduced. In the next subsection, the numerical simulations for the half-vehicle model with flexible vehicle body are restricted to the case where the time delay is not taken into account.

Based on the above validation and analysis, considering the fact that we utilized the same objective function, vehicle system model and LQG algorithm as those used by Hac [12], we can conclude that the numerical results offered by Hac in [12] are not correct.

5.2.3 Results and discussion. In this subsection, for the half-vehicle model with flexible vehicle body and without the time delay between front and rear road inputs, the numerical simulation results based on the A-i-O method are compared with those based on the LQG algorithm. As will be seen, the optimized vehicle system derived from the A-i-O method is superior to that based on the LQG algorithm in the aspects of ride comfort, suspension working spaces and unsprung mass dynamic loads with almost the same power consumption.

In the A-i-O method case, it is assumed that: the vehicle system parameters EI, ρA, c_3 and c_4 take their nominal values; M, m_1, m_2, I_c, k_3, k_4, a_1 ($a_1 = a_2$) and b_2 ($b_2 = L - b_1$) are permitted to vary by 10% from their nominal values; k_1, k_2, c_1 and c_2 are allowed to change by 50% from their nominal values; and the standard deviations of the sensors' random errors are taken as 0.06 m/s. The nominal system parameters are listed in table A2. The vehicle speed and the random road characteristic parameters are assigned the values offered in the last subsection. Based on the calculation offered in the last subsection, the weighting factors are set as: $\rho_1 = 10^{-8}$, $\rho_2 = 1$, $\rho_3 = 10^5$, and $\rho_4 = 10^4$. By using the A-i-O method, we can obtain the optimal design variables for the half-vehicle model with a flexible vehicle body as listed in table 8. For the purpose of comparison, the corresponding nominal values for these design variables are also provided in the table. The obtained optimal feedback control gain matrix based on the A-i-O together with that based on the LQG are also offered in table 9. Note that, in the LQG case, the simulation condition is the same as that of the A-i-O case except that the passive vehicle system parameters take their nominal values.

Numerical experiments show that the optimized values of the design variables shown in table 8 are almost independent of the weighting factor ρ_1 by using the A-i-O method. Thus, with $\rho_2 = 1$, $\rho_3 = 10^5$, and $\rho_4 = 10^4$, no matter what the extent of the actuator forces in the secondary suspensions, the optimized vehicle system parameters shown in table 8 are almost the same when the vehicle dynamic system, estimator and controller are optimized simultaneously using the A-i-O method.

Figure 12 shows the dependence of the index (J) and its parts (J_1, J_2, J_3, J_4) upon the weighting factor ρ_1; figure 13 illustrates the trade-off solutions of weighted root of mean square (RMS) vertical body acceleration and weighted RMS wheel dynamic load; figure 14 offers the the trade-off solutions of weighted RMS vertical body acceleration and weighted RMS suspension working space. Note that the weighted RMS vertical body acceleration, unsprung mass dynamic load and suspension working space are based on the performance terms J_2, J_3 and J_4, respectively.

Table 8. Optimized values for vehicle system design variables.

	m_1 (kg)	m_2 (kg)	M (kg)	I_c (kg m^2)	a_1 (m)	b_2 (m)
NV†	1.0×10^3	1.0×10^3	1.0×10^4	1.2×10^5	4.0	2.0
A-i-O	900.0	900.0	1.1×10^4	1.32×10^5	3.60	1.92
	k_1 (N/m)	c_1 (N/m/s)	k_2 (N/m)	c_2 (N/m/s)	k_3 (N/m)	k_4 (N/m)
NV	2.0×10^5	2.0×10^4	2.0×10^5	2.0×10^4	2.0×10^6	2.0×10^6
A-i-O	1.258×10^5	2.035×10^4	2.134×10^5	2.767×10^4	1.8×10^6	1.8×10^6

†Nominal values.

Downloaded by [Kungliga Tekniska Hogskola] at 04:36 26 November 2015

Table 9. Feedback control gain matrix for optimal suspensions.

	$K_{1,1} \times 10^{-5}$	$K_{1,2} \times 10^{-5}$	$K_{1,3} \times 10^{-4}$	$K_{1,4} \times 10^{-5}$	$K_{1,5} \times 10^{-5}$	$K_{1,6} \times 10^{-4}$	$K_{1,7} \times 10^{-5}$
A-i-O	9.6089	−5.6295	6.6631	9.4087	−7.9097	−4.8001	6.7035
LQG	4.5908	1.1374	10.3630	2.7474	−2.0241	−2.4724	1.3482
	$K_{1,8} \times 10^{-4}$	$K_{1,9} \times 10^{-7}$	$K_{1,10} \times 10^{-5}$	$K_{1,11} \times 10^{-8}$	$K_{1,12} \times 10^{-7}$	$K_{1,13} \times 10^{-8}$	$K_{1,14} \times 10^{-7}$
A-i-O	3.2283	−1.0010	−0.9183	5.6463	1.0728	−1.9243	−0.3944
LQG	−0.9422	−1.6119	−1.5065	1.8915	0.3613	−5.8641	−1.1726
	$K_{2,1} \times 10^{-5}$	$K_{2,2} \times 10^{-5}$	$K_{2,3} \times 10^{-5}$	$K_{2,4} \times 10^{-5}$	$K_{2,5} \times 10^{-5}$	$K_{2,6} \times 10^{-4}$	$K_{2,7} \times 10^{-5}$
A-i-O	−5.6309	8.7313	0.5922	−9.1449	6.7078	3.2284	−7.9004
LQG	1.1373	4.5908	1.0363	−2.7474	1.3482	−0.9422	−2.0241
	$K_{2,8} \times 10^{-4}$	$K_{2,9} \times 10^{-7}$	$K_{2,10} \times 10^{-5}$	$K_{2,11} \times 10^{-8}$	$K_{2,12} \times 10^{-7}$	$K_{2,13} \times 10^{-8}$	$K_{2,14} \times 10^{-7}$
A-i-O	−4.0671	−1.0019	−0.9506	−5.6463	−1.0724	−1.9240	−0.3936
LQG	−2.4724	−1.6119	−1.5065	−1.8915	−0.3613	−5.8641	−1.1726

Downloaded by [Kungliga Tekniska Hogskola] at 04:36 26 November 2015

Investigation of figures 12, 13, and 14 demonstrates that the overall performance of the active suspensions based on the A-i-O method is superior to that based on the LQG. The active suspensions based on the A-i-O method achieves the overall performance improvement at the expense of using larger control forces than those based on the LQG. However, under the above simulation conditions, the total average control power consumption for the A-i-O based active suspensions is just 1.4% higher than that (3.1896 kW) required for the LQG based active suspensions. The reason for this phenomenon is that although the actuators for the A-i-O based suspensions use larger control forces, the relative motions between the sprung mass and the unsprung masses are better controlled than those of the LQG based suspensions.

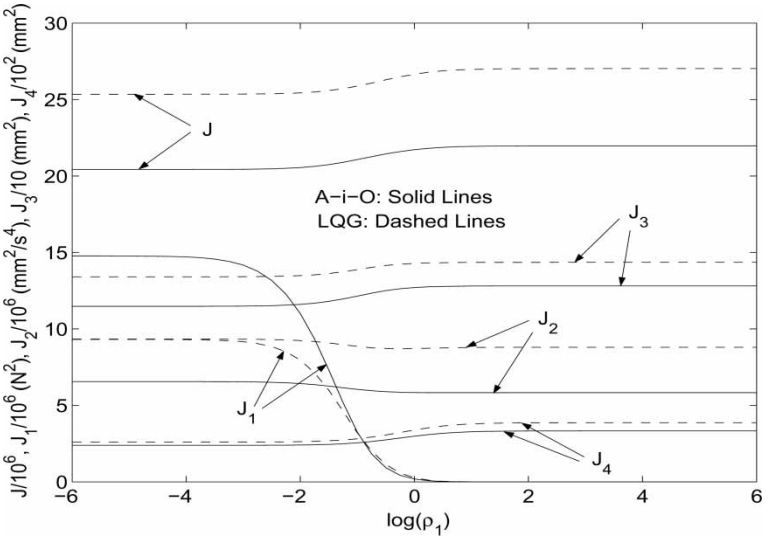

Figure 12. Performance index J and its parts J_1, J_2, J_3, and J_4 versus ρ_1.

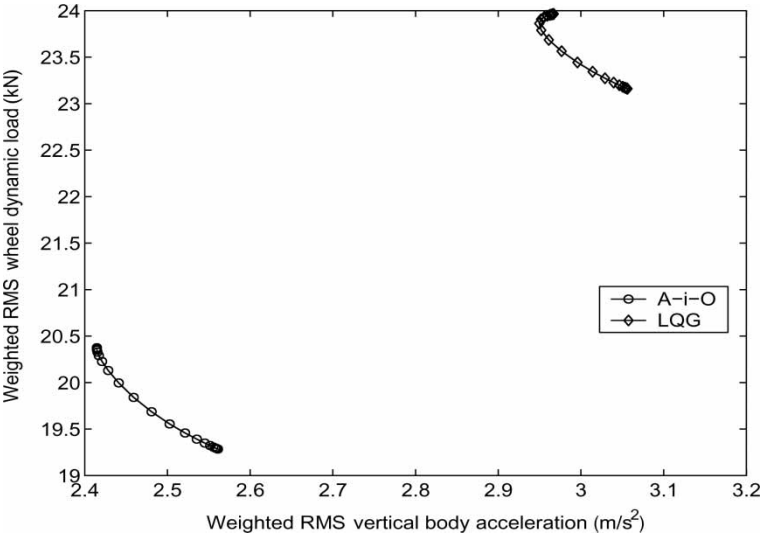

Figure 13. RMS trade-off solutions of vertical body acceleration versus unsprung mass dynamic load.

Thus, the rectified average piston velocities of the actuators for the A-i-O based suspensions are lower than those of the actuators for the LQG based suspensions and the amounts of total average control power consumption for both cases are almost the same. Figure 15 provides the relationship between vehicle speed and control power consumption.

Based on equation (39), the filtering error covariance matrix **P** depends on the sensor accuracy due to **R** in equation (36) and the sensor arrangement due to $\mathbf{C}_a$ in equation (35). According to equation (40), as mentioned previously, the performance index J_{opt} contains two parts. The first part, J_Q, arises because of the random road excitations; the second part, J_r, results from inexact state estimation due to the existence of the matrix **P**. J_r vanishes when **P** vanishes. Thus, the two factors, the sensor accuracy and the sensor arrangement, influence J,

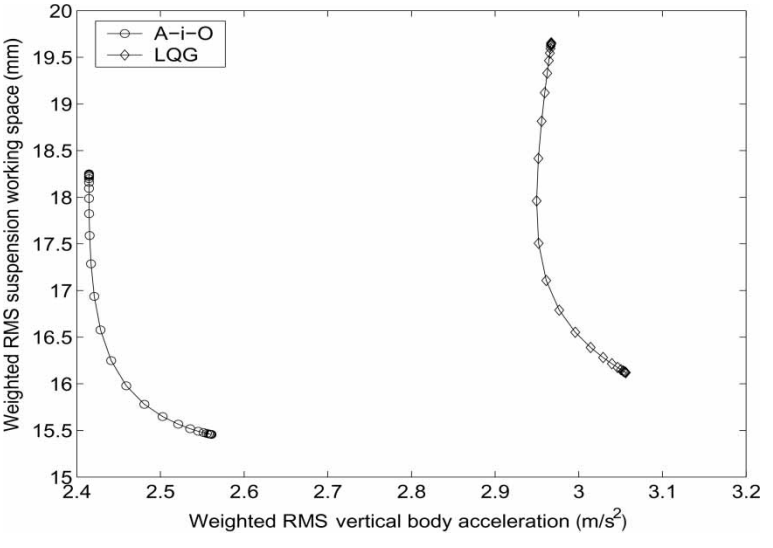

Figure 14. RMS trade-off solutions of vertical body acceleration versus suspension working space.

Downloaded by [Kungliga Tekniska Hogskola] at 04:36 26 November 2015

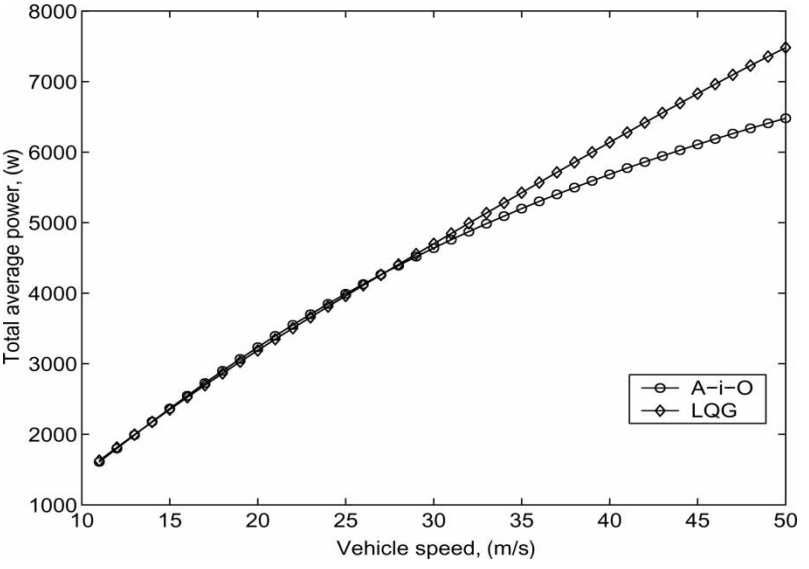

Figure 15. Total average control power consumption versus vehicle speed.

J_r, and **P**. Figure 16 shows the effect of sensor errors on J, J_r and **P** for both the A-i-O based active suspensions and the LQG based active suspensions. Note that the results in figure 16 are based on the sensor arrangement with five sensors measuring the vertical velocities of the front and rear unsprung masses and the vertical velocities at the three vehicle body points, i.e., the rear end, the front end and the middle point.

It is obvious that in both the A-i-O and the LQG cases, as sensor errors increase, J, J_r and $trace(\mathbf{P})$ increase. Over the sensor error range offered, the J and $trace(\mathbf{P})$ based on the A-i-O method are smaller than those based on the LQG algorithm, respectively. However, over the lower sensor error value range, the J_r based on the LQG algorithm is smaller than

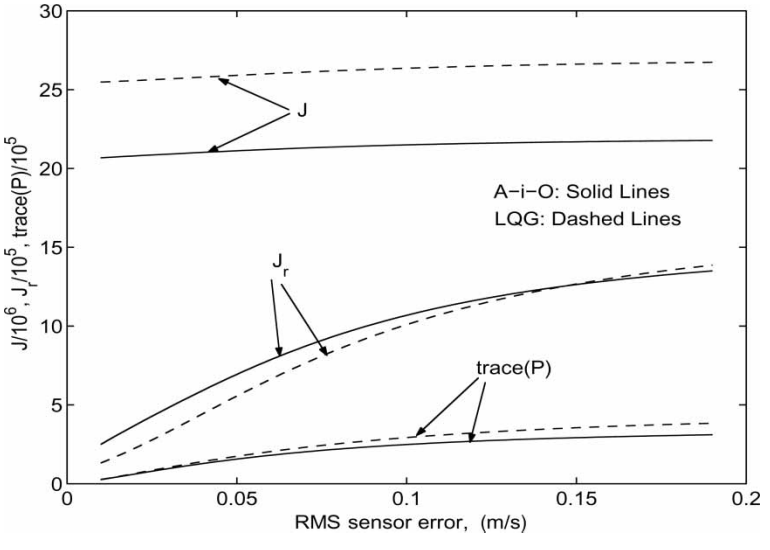

Figure 16. Effect of RMS sensor errors on performance indices J, J_r, and $trace(\mathbf{P})$.

Downloaded by [Kungliga Tekniska Hogskola] at 04:36 26 November 2015

Downloaded by [Kungliga Tekniska Hogskola] at 04:36 26 November 2015

that based on the A-i-O method. The reason for the phenomenon is that J_r depends not only on the filtering error covariance matrix **P** but also on the control feedback gain matrix **K** and weighting matrix **H** (see equation (40)).

To investigate the influence of sensor arrangement on the state estimation, different sensor arrangements are used in this research. For all the sensor arrangements, two sensors are used to measure the vertical velocities of the front and rear unsprung masses. Numerical experiments show that among all possible combinations of locations for two sensors for measuring the vehicle body vertical velocities, the optimal plan with minimal J_r is the one that the two sensors are located at the front end and the rear end of the vehicle body, respectively. With the third sensor introduced, the best location is the middle of the vehicle body. This sensor arrangement is consistent with what Hac [12] found: 'the body motion consists mainly of vibration connected with the lowest mode and to minimize measurement errors the sensors should be located at extreme points of the functions of these mode shapes'. Figure 17 offers the relationship between J_r and weighting factor ρ_1 in the A-i-O case when four and five sensors are used with the above optimal arrangements. With the additional sensor located at the middle of the vehicle body, the value of J_r is lower than that for the four sensor arrangement over the lower ρ_1 value range within which the active suspensions take effect.

To examine the behaviour of the A-i-O based active suspensions (optimized without the Kalman filters at 20.0 m/s) at other speeds, the performance indices of acceleration, unsprung mass dynamic deflection and suspension working space based on the A-i-O are compared with those based on the LQG. Figure 18 illustrates the dependence of these performance indices on vehicle speed. Results shown in figure 18 together with those offered in figure 15 demonstrate that the optimized vehicle system based on the A-i-O method is better controlled than that based on the LQG algorithm in vertical acceleration, unsprung mass dynamic load and suspension working space with almost the same control power consumption over the lower speed range and with less control power consumption within the higher speed range. It should be noted that the optimized vehicle system based on the A-i-O method achieves the above improvements even though its vehicle body mass (M) is 10% larger than its nominal value.

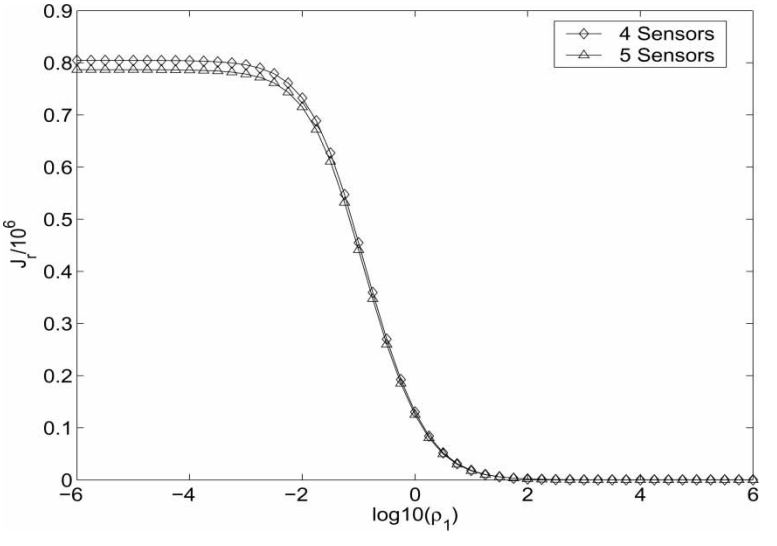

Figure 17. Effect of sensor arrangement on J_r.

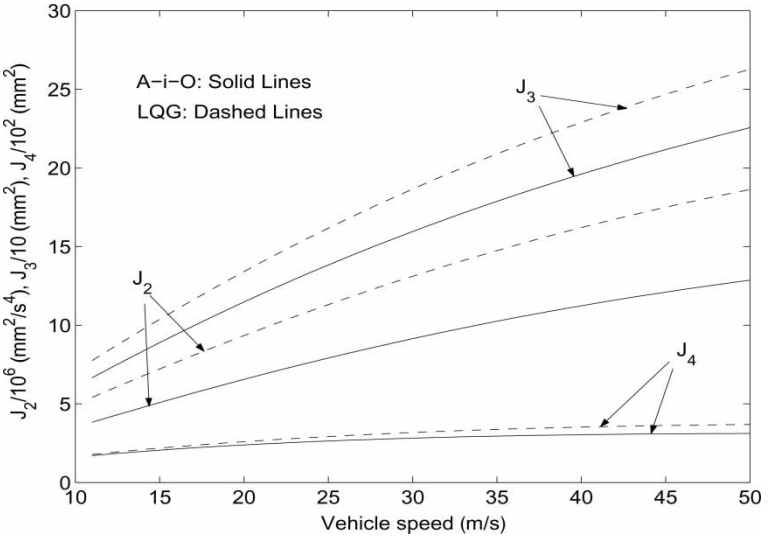

Figure 18. Performance indices of acceleration, unsprung mass dynamic deflection, and suspension working space as a function of vehicle velocity.

6. Conclusions

A methodology for the design of mechatronic vehicles was proposed and developed in this study. The methodology has the following features: (1) multidisciplinary optimization (MDO) methods are introduced to integrate strongly coupled mechanical, control and measurement subsystems associated with vehicle performance; (2) with the scalarization technique, a vector optimization problem is converted into a scalar one; and (3) with genetic algorithms (GAs) and other effective search algorithms, the coupled subsystems are optimized simultaneously.

Numerical experiments demonstrated the feasibility and efficacy of the proposed design methodology for resolving conflicting design requirements of mechatronic vehicles. This methodology is suitable for the design of mechatronic vehicles where: (1) there is interaction between different vehicle subsystems or analysis disciplines; (2) there are multiple design criteria; (3) there are multiple local optima; (4) there are multiple design variables; (5) no matter whether the scalar objective function is continuous or discontinuous, there is no need for sensitivity analysis for the system solver or the GA. The limitation of the application of the methodology is that the associated computational burden is heavy. However, parallel processing, for which the methodology is ideally suited, could be used for reducing the computer time required for the design optimization.

The methodology is applied to the design of mechatronic vehicles with active suspensions. In the design, the All-in-One (A-i-O) multidisciplinary optimization method was used to integrate GAs, multibody dynamics, the LQG control strategy and the Kalman filter algorithm. By resolving the conflicting requirements for ride comfort, suspension working spaces and unsprung mass dynamic loads, half-vehicle models with passive and active suspensions were optimally designed. In the simulations, both random and deterministic road inputs, both rigid and flexible vehicle body and both perfect measurement of full state variables and limited state variables with Kalman filter cases are considered. The time domain analysis and a systematic covariance analysis are carried out.

Numerical results show that the optimized vehicle systems based on the A-i-O method have better overall performance than that derived using the LQG algorithm not only in ride comfort

Downloaded by [Kungliga Tekniska Hogskola] at 04:36 26 November 2015

and suspension working spaces, but also in unsprung mass dynamic loads with almost the same control power consumption over lower speed range and less control power consumption within higher speed range. The simulation results based on the simple quarter-vehicle model can be used not only to analyse the vehicle dynamic behaviour qualitatively but also to validate the simulation results based on complex vehicle models. With the co-existence of passive and active components in vehicle suspensions and the design variables determined by using the A-i-O method, the corresponding actuator forces can actively resist road disturbances much longer than the actuator forces based on the case where the corresponding suspensions have no passive elements and the design variables are determined by using the LQG algorithm. Although the vehicle system is optimized at a specified vehicle speed based on the A-i-O method, the resulting overall vehicle performance is still superior to that based on the LQG algorithm over a regular speed range.

Downloaded by [Kungliga Tekniska Hogskola] at 04:36 26 November 2015

Acknowledgements

Financial support of this research by the Natural Sciences and Engineering Research Council of Canada and Bombardier Inc. is gratefully acknowledged. The authors would also like to thank Professor Ron Anderson at Queens University, Canada, for providing the A'GEM software. Finally, the authors thank the three anonymous reviewers for their constructive comments on the paper.

References

[1] Pil, A. and Asada, H., 1996, *IEEE/ASME Transactions on Mechatronics* **1**, 191–203.
[2] Suzuki, S. and Kawamura, N., 1996, *Journal of Aircraft*, **33**, 567–571.
[3] Bestle, D., 1994, Optimization of Automotive Systems. In E.J. Haug (Ed), *Concurrent Engineering: Tools and Technologies for Mechanical System Design*, (Berlin: Springer-Verlag), pp. 274–296.
[4] Schiehlen, W., 1994, Symbolic Computations in Multibody Systems. In M. Pereira and J. Ambrosio (Eds) *Computer–Aided Analysis of Rigid and Flexible Mechanical Systems*, pp. 101–136.
[5] Bestle, D., Eberhard, P., and Schiehlem, W., 1995, *Journal of Computer and Systems and Sciences International*, **33**, 7–15.
[6] Baumal, A., McPhee, J., and Calamai, P., 1998, *Comp. Meth. Appl. Mech. Eng.*, **163**, 87–94.
[7] He, Y. and McPhee, J., 2002, *Vehicle System Dynamics*, **37** Supplement, 397–408.
[8] Karnopp, D., 1990, *ASME J. Dyn. Sys. Meas. Cont.*, **112**, 448–455.
[9] Thompson, A., 1976, *Vehicle System Dynamics*, **5**, 187–203.
[10] Thompson, A. and Pearce, C., 1979, SAE Paper No. 790478.
[11] Hac, A., 1985, *Journal of Sound and Vibration*, **100**(3), 343–357.
[12] Hac, A., 1986, *ASME J. Dyn. Sys. Meas. Cont.*, **108**, 106–110.
[13] He, Y. and McPhee, J., 2002, An Integrated Approach Using Genetic Algorithms, Multibody Dynamics, and LQG Control for Design Optimization of Ground Vehicles with Active Suspensions. CD-ROM Proceedings of CSME Forum, Queen's University, Canada, 2002.
[14] He, Y. and McPhee, J., 2005, *Journal of Sound and Vibration*, **283**, 217–241.
[15] Anderson, R., 1993, *Vehicle System Dynamics*, **22**, 41–44.
[16] Langlois, R., Hanna, D. and Anderson, R., 1991, *Vehicle System Dynamics*, **20**, 340–353.
[17] Alleyne, A., Neuhaus, P. and Hedrick, J., 1993, *Vehicle System Dynamics*, **22**, 309–320.
[18] Hrovat, D., 1993, *ASME J. Dyn. Sys. Meas. Cont.*, **115**(2B), 328–342.
[19] Kodiyalam, S. and Sobieski, J., 2001, *Int. J. Vehicle Design*, **25**(1/2), 3–22.
[20] Eberhard, P., Schiehlen, W. and Bestle, D., 1999, *Archive of Applied Mechanics*, **69**, 543–554.
[21] Bestle, D. and Eberhard, P., 1995, Dynamic System Design via Multicriteria Optimization. In G. Fandel and T. Gal (Eds) *Multiple Criteria Decision Making: Proceedings of the 12th International Conference on Multiple Criteria Decision Making*, (Berlin: Springer-Verlag), pp. 467–478.
[22] He, Y. and McPhee, J., *Multibody System Dynamics*, in press.
[23] Cramer, E., Dennis, J., Frank, P., Lewis, R. and Shubin, G., 1994, *SIAM Journal on Optimization*, **4**, 754–776.
[24] Alleyne, A. and Hedrick, J.K., 1995, *IEEE Transactions on Control Systems Technology*, **3**(1), 94–101.
[25] Alleyne, A. and Liu, R., 1999, *ASME J. Dyn. Sys. Meas. Cont.*, **121**(2), 184–190.
[26] Hady, M. and Crolla, D., 1992, *Int. J. Vehicle Design*, **13**(2), 144–158.
[27] Sinha, P., Wormley, D. and Hedrick, J., 1978, *ASME J. Dyn. Sys. Means. Cont.*, **100**, 270–283.
[28] He, Y., 2003, Design of Rail Vehicles with Passive and Active Suspensions Using Multidisciplinary Optimization, Multibody Dynamics, and Genetic Algorithms. Ph.D. Thesis, University of Waterloo, Canada, 2003.

[29] Foo, D. and Goodall, R., 2003, *Control Engineering Practice*, **8**, 507–518.
[30] Hedrick, J. and Firouztash, H., 1974, *IEEE Trans. on Automatic Control*, **AC-19**(4), 587–589.
[31] Louam, N., Wilson, D. and Sharp, R., 1998, *Vehicle System Dynamics*, **17**, 317–336.
[32] Elmadany, M., 1988, *Vehicle System Dynamics*, **17**, 193–210.
[33] Heal, K., Hansen, M. and Richard, K., 1998, *Maple V Learning Guide* (New York: Springer).
[34] Goldberg, D.E., 1989, *Genetic Algorithms in Search, Optimization, and Machine Learning* (New York: Addison-Wesley).
[35] Whitley, D., 1989, The Genetic Algorithm and Selection Pressure: Why Rank-Based Allocation of Reproduction Trials Is Best. In J.D. Schaffer (Ed), *Proceeding of the Third International Conference on Genetic Algorithms*. George Mason University, VA, USA, Morgan Kaufmann Publishers, 1989, pp. 116–121.
[36] Eberhard, P., Dignath, F. and Kubler, L., 2003, *Multibody System Dynamics*, **9**, 143–164.

Downloaded by [Kungliga Tekniska Hogskola] at 04:36 26 November 2015

Appendix

Half-vehicle model system parameters

The vehicle system parameters for the half-vehicle models with rigid vehicle body and flexible vehicle body are shown in the following tables.

Half-vehicle model dynamic system matrices

Rigid vehicle body case.

$$\mathbf{A} = \begin{bmatrix} 0 & 0 & 0 & 0 & 1 & 0 & 0 & 0 \\ 0 & 0 & 0 & 0 & 0 & 1 & 0 & 0 \\ 0 & 0 & 0 & 0 & 0 & 0 & 1 & 0 \\ 0 & 0 & 0 & 0 & 0 & 0 & 0 & 1 \\ -\dfrac{k_1+k_3}{m_1} & \dfrac{k_1}{m_1} & 0 & 0 & -\dfrac{c_1+c_3}{m_1} & \dfrac{c_1}{m_1} & 0 & 0 \\ \dfrac{k_1 M_{11}}{I_c M} & \dfrac{-k_1 M_{11}}{I_c M} & \dfrac{-k_2 M_{12}}{I_c M} & \dfrac{k_2 M_{12}}{I_c M} & \dfrac{c_1 M_{11}}{I_c M} & \dfrac{-c_1 M_{11}}{I_c M} & \dfrac{-c_2 M_{12}}{I_c M} & \dfrac{c_2 M_{12}}{I_c M} \\ 0 & 0 & -\dfrac{k_2+k_4}{m_2} & \dfrac{k_2}{m_2} & 0 & 0 & -\dfrac{c_2+c_4}{m_2} & \dfrac{c_2}{m_2} \\ \dfrac{-k_1 M_{12}}{I_c M} & \dfrac{k_1 M_{12}}{I_c M} & \dfrac{k_2 M_{22}}{I_c M} & \dfrac{-k_2 M_{22}}{I_c M} & \dfrac{-c_1 M_{12}}{I_c M} & \dfrac{c_1 M_{12}}{I_c M} & \dfrac{c_2 M_{22}}{I_c M} & \dfrac{-c_2 M_{22}}{I_c M} \end{bmatrix} \tag{A1}$$

Table A1. Nominal vehicle system parameters for the half-vehicle model with rigid vehicle body [10].

Inertial property parameters	Geometric parameters	Primary suspension parameters	Secondary suspension parameters
$M = 505.1$ (kg)	$L = 2.5654$ (m)	$k_3 = 155.9$ (kN/m)	$k_1 = 19.96$ (kN/m)
$m_1 = 28.58$ (kg)	$b_1 = 2.5654$ (m)	$c_3 = 0.0$ (N/m/s)	$c_1 = 2014.0$ (kN/m/s)
$m_2 = 54.43$ (kg)	$b_2 = 0.0$ (m)	$k_4 = 155.9$ (kN/m)	$k_2 = 22.59$ (kN/m)
$I_c = 651.0$ (kg m^2)	$a_1 = 1.0978$ (m)	$c_4 = 0.0$ (N/m/s)	$c_2 = 2082.0$ (kN/m/s)
	$a_2 = 1.4676$ (m)		

Table A2. Nominal vehicle system parameters for the half-vehicle model with flexible vehicle body [12].

Inertial property parameters	Geometric parameters	Primary suspension parameters	Secondary suspension parameters
$M = 10^4$ (kg)	$L = 12.0$ (m)	$k_3 = 2000.0$ (kN/m)	$k_1 = 200.0$ (kN/m)
$m_1 = 10^3$ (kg)	$b_1 = 2.0$ (m)	$c_3 = 0.0$ (N/m/s)	$c_1 = 20$ (kN/m/s)
$m_2 = 10^3$ (kg)	$b_2 = 2.0$ (m)	$k_4 = 2000.0$ (kN/m)	$k_2 = 200.0$ (kN/m)
$I_c = 1.2 \times 10^5$ (kg m^2)	$a_1 = 4.0$ (m)	$c_4 = 0.0$ (N/m/s)	$c_2 = 20.0$ (kN/m/s)
$EI = 10^8$ (N m^2)	$a_2 = 4.0$ (m)		
$\rho A = 834.0$ (kg/m)			

Downloaded by [Kungliga Tekniska Hogskola] at 04:36 26 November 2015

where $M_{11} = a_1^2 M + I_c$, $M_{12} = a_1 a_2 M - I_c$, $M_{22} = a_2^2 M + I_c$.

$$\mathbf{B} = \begin{bmatrix} 0 & 0 & 0 & 0 & -1/m_1 & 1/M + a_1^2/I_c & 0 & 1/M - a_1 a_2/I_c \\ 0 & 0 & 0 & 0 & 0 & 1/M - a_1 a_2/I_c & -1/m_2 & 1/M + a_2^2/I_c \end{bmatrix}^T \tag{A2}$$

$$\mathbf{C} = \begin{bmatrix} 1 & 0 & 0 & 0 & 0 & 0 & 0 & 0 \\ 0 & 1 & 0 & 0 & 0 & 0 & 0 & 0 \\ 0 & 0 & 1 & 0 & 0 & 0 & 0 & 0 \\ 0 & 0 & 0 & 1 & 0 & 0 & 0 & 0 \end{bmatrix} \tag{A3}$$

$$\mathbf{D} = \begin{bmatrix} -1 & -1 & 0 & 0 & c_3/m_1 & 0 & 0 & 0 \\ 0 & 0 & -1 & -1 & 0 & 0 & c_4/m_2 & 0 \end{bmatrix}^T. \tag{A4}$$

Flexible vehicle body case. For convenience, it is assumed that the matrix $\mathbf{A}$ is divided into two sub-matrices $\mathbf{A}_1$ and $\mathbf{A}_2$ as follows

$$\mathbf{A} = \begin{bmatrix} \mathbf{A}_1 & \mathbf{A}_2 \end{bmatrix} \tag{A5}$$

where sub-matrices $\mathbf{A}_1$ and $\mathbf{A}_2$ can be further expressed as:

$$\mathbf{A}_1 = \begin{bmatrix} 0 & 0 & A_{1,3} & A_{1,4} & 0 & A_{1,6} & 0 \\ 0 & 0 & A_{2,3} & A_{2,4} & 0 & 0 & 0 \\ A_{3,1} & A_{3,2} & A_{3,3} & A_{3,4} & 0 & A_{3,6} & 0 \\ A_{4,1} & A_{4,2} & A_{4,3} & A_{4,4} & 0 & A_{4,6} & 0 \\ 0 & 0 & 0 & 0 & 0 & A_{5,6} & 0 \\ A_{6,1} & 0 & A_{6,3} & A_{6,4} & A_{6,5} & A_{6,6} & 0 \\ 0 & 0 & 0 & 0 & 0 & 0 & 0 \\ 0 & A_{8,2} & A_{8,3} & A_{8,4} & 0 & 0 & A_{8,7} \\ 0 & 0 & 0 & 0 & 0 & 0 & 0 \\ A_{10,1} & A_{10,2} & A_{10,3} & A_{10,4} & 0 & A_{10,6} & 0 \\ 0 & 0 & 0 & 0 & 0 & 0 & 0 \\ A_{12,1} & A_{12,2} & A_{12,3} & A_{12,4} & 0 & A_{12,6} & 0 \\ 0 & 0 & 0 & 0 & 0 & 0 & 0 \\ A_{14,1} & A_{14,2} & A_{14,3} & A_{14,4} & 0 & A_{14,6} & 0 \end{bmatrix} \tag{A6}$$

$$\mathbf{A}_2 = \begin{bmatrix} 0 & 0 & A_{1,10} & 0 & A_{1,12} & 0 & A_{1,14} \\ A_{2,8} & 0 & A_{2,10} & 0 & A_{2,12} & 0 & A_{2,14} \\ A_{3,8} & 0 & A_{3,10} & 0 & A_{3,12} & 0 & A_{3,14} \\ A_{4,8} & 0 & A_{4,10} & 0 & A_{4,12} & 0 & A_{4,14} \\ 0 & 0 & 0 & 0 & 0 & 0 & 0 \\ 0 & 0 & A_{6,10} & 0 & A_{6,12} & 0 & A_{6,14} \\ A_{7,8} & 0 & 0 & 0 & 0 & 0 & 0 \\ A_{8,8} & 0 & A_{8,10} & 0 & A_{8,12} & 0 & A_{8,14} \\ 0 & 0 & A_{9,10} & 0 & 0 & 0 & 0 \\ A_{10,8} & A_{10,9} & A_{10,10} & 0 & A_{10,12} & 0 & A_{10,14} \\ 0 & 0 & 0 & 0 & A_{11,12} & 0 & 0 \\ A_{12,8} & 0 & A_{12,10} & A_{12,11} & A_{12,12} & 0 & A_{12,14} \\ 0 & 0 & 0 & 0 & 0 & 0 & A_{13,14} \\ A_{14,8} & 0 & A_{14,10} & 0 & A_{14,12} & A_{14,13} & A_{14,14} \end{bmatrix} \tag{A7}$$

where the elements of matrices $\mathbf{A}_1$ and $\mathbf{A}_2$ are given as: $A_{1,3} = 1$, $A_{1,4} = a_1$, $A_{1,6} = -1$, $A_{1,10} = Z_1(b_1)$, $A_{1,12} = Z_2(b_1)$, $A_{1,14} = Z_3(b_1)$, $A_{2,3} = 1$, $A_{2,4} = -a_2$, $A_{2,8} = -1$, $A_{2,10} = Z_1(b_2)$, $A_{2,12} = Z_2(b_2)$, $A_{2,14} = Z_3(b_2)$, $A_{3,1} = -k_1/M$, $A_{3,2} = -k_2/M$, $A_{3,3} = -(c_1 + c_2)/M$, $A_{3,4} = -(a_1c_1 - a_2c_2)/M$, $A_{3,6} = c_1/M$, $A_{3,8} = c_2/M$, $A_{3,10} = -(c_1Z_1(b_1) + c_2Z_1(b_2))/M$, $A_{3,12} = -(c_1Z_2(b_1) + c_2Z_2(b_2))/M$, $A_{3,14} = -(c_1Z_3(b_1) + c_2Z_3(b_2))/M$, $A_{4,1} = -a_1k_1/I_c$, $A_{4,2} = a_2k_2/I_c$, $A_{4,3} = -(a_1c_1 - a_2c_2)/I_c$, $A_{4,4} = -(a_1^2c_1 + a_2^2c_2)/I_c$, $A_{4,6} = a_1c_1/I_c$, $A_{4,8} = -a_2c_2/I_c$, $A_{4,10} = -(a_1c_1Z_1(b_1) - a_2c_2Z_1(b_2))/I_c$, $A_{4,12} = -(a_1c_1Z_2(b_1) - a_2c_2Z_2(b_2))/I_c$, $A_{4,14} = -(a_1c_1Z_3(b_1) - a_2c_2Z_3(b_2))/I_c$, $A_{5,6} = 1$, $A_{6,1} = k_1/m_1$, $A_{6,3} = c_1/m_1$, $A_{6,4} = a_1c_1/m_1$, $A_{6,5} = -k_3/m_1$, $A_{6,6} = -(c_1 + c_3)/m_1$, $A_{6,10} = c_1Z_1(b_1)/m_1$, $A_{6,12} = c_1Z_2(b_1)/m_1$, $A_{6,14} = c_1Z_3(b_1)/m_1$, $A_{7,8} = 1$, $A_{8,2} = k_2/m_2$, $A_{8,3} = c_2/m_2$, $A_{8,4} = -a_2c_2/m_2$, $A_{8,7} = -k_4/m_2$, $A_{8,8} = -(c_2 + c_4)/m_2$, $A_{8,10} = c_2Z_1(b_2)/m_2$, $A_{8,12} = c_2Z_2(b_2)/m_2$, $A_{8,14} = c_2Z_3(b_2)/m_2$, $A_{9,10} = 1$, $A_{10,1} = -k_1Z_1(b_1)/M_1$, $A_{10,2} = -k_2Z_1(b_2)/M_1$, $A_{10,3} = -(c_1Z_1(b_1) + c_2Z_1(b_2))/M_1$, $A_{10,4} = -(a_1c_1Z_1(b_1) - a_2c_2Z_1(b_2))/M_1$, $A_{10,6} = c_1Z_1(b_1)/M_1$, $A_{10,8} = c_2Z_1(b_2)/M_1$, $A_{10,9} = -\gamma_1/M_1$, $A_{10,10} = -(\vartheta\gamma_1 + c_1Z_1^2(b_1) + c_2Z_1^2(b_2))/M_1$, $A_{10,12} = -(c_1Z_1(b_1)Z_2(b_1) + c_2Z_1(b_2)Z_2(b_2))/M_1$, $A_{10,14} = -(c_1Z_1(b_1)Z_3(b_1) + c_2Z_1(b_2)Z_3(b_2))/M_1$, $A_{11,12} = 1$, $A_{12,1} = -k_1Z_2(b_1)/M_2$, $A_{12,2} = -k_2Z_2(b_2)/M_2$, $A_{12,3} = -(c_1Z_2(b_1) + c_2Z_2(b_2))/M_2$, $A_{12,4} = -(a_1c_1Z_2(b_1) - a_2c_2Z_2(b_2))/M_2$, $A_{12,6} = c_1Z_2(b_1)/M_2$, $A_{12,8} = c_2Z_2(b_2)/M_2$, $A_{12,10} = -(c_1Z_1(b_1)Z_2(b_1) + c_2Z_1(b_2)Z_2(b_2))/M_2$, $A_{12,11} = -\gamma_2/M_2$, $A_{12,12} = -(\vartheta\gamma_2 + c_1Z_2^2(b_1) + c_2Z_2^2(b_2))/M_2$, $A_{12,14} = -(c_1Z_2(b_1)Z_3(b_1) + c_2Z_2(b_2)Z_3(b_2))/M_2$, $A_{13,14} = 1$, $A_{14,1} = -k_1Z_3(b_1)/M_3$, $A_{14,2} = -k_2Z_3(b_2)/M_3$, $A_{14,3} = -(c_1Z_3(b_1) + c_2Z_3(b_2))/M_3$, $A_{14,4} = -(a_1c_1Z_3(b_1) - a_2c_2Z_3(b_2))/M_3$, $A_{14,6} = c_1Z_3(b_1)/M_3$, $A_{14,8} = c_2Z_3(b_2)/M_3$, $A_{14,10} = -(c_1Z_1(b_1)Z_3(b_1) + c_2Z_1(b_2)Z_3(b_2))/M_3$, $A_{14,12} = -(c_1Z_2(b_1)Z_3(b_1) + c_2Z_2(b_2)Z_3(b_2))/M_3$, $A_{14,13} = -\gamma_3/M_3$, $A_{14,14} = -(\vartheta\gamma_3 + c_1Z_3^2(b_1) + c_2Z_3^2(b_2))/M_3$.

Again it is assumed that the matrix $\mathbf{B}$ takes the following format

$$\mathbf{B} = \begin{bmatrix} \mathbf{B}_1 & \mathbf{B}_2 \end{bmatrix}^T \tag{A8}$$

where the matrices $\mathbf{B}_1$ and $\mathbf{B}_2$ are expressed as follows

$$\begin{cases} \mathbf{B}_1 = \begin{bmatrix} 0 & 0 & 1/M & a_1/I_c & 0 & -1/m_1 & 0 \\ 0 & 0 & 1/M & -a_2/I_c & 0 & 0 & 0 \end{bmatrix} \\ \mathbf{B}_2 = \begin{bmatrix} 0 & 0 & Z_1(b_1)/M_1 & 0 & Z_2(b_1)/M_2 & 0 & Z_3(b_1)/M_3 \\ -1/m_2 & 0 & Z_1(b_2)/M_1 & 0 & Z_2(b_2)/M_2 & 0 & Z_3(b_2)/M_3 \end{bmatrix} \end{cases}. \tag{A9}$$

Downloaded by [Kungliga Tekniska Hogskola] at 04:36 26 November 2015

The disturbance matrices $\mathbf{D}_1$ and $\mathbf{D}_2$ are of the following forms

$$\mathbf{D}_1 = \begin{bmatrix} 0 & 0 & 0 & 0 & 0 & k_3/m_1 & 0 & 0 & 0 & 0 & 0 & 0 & 0 & 0 \\ 0 & 0 & 0 & 0 & 0 & 0 & 0 & k_4/m_2 & 0 & 0 & 0 & 0 & 0 & 0 \end{bmatrix} \tag{A10}$$

$$\mathbf{D}_2 = \begin{bmatrix} 0 & 0 & 0 & 0 & 0 & c_3/m_1 & 0 & 0 & 0 & 0 & 0 & 0 & 0 & 0 \\ 0 & 0 & 0 & 0 & 0 & 0 & 0 & c_4/m_2 & 0 & 0 & 0 & 0 & 0 & 0 \end{bmatrix}. \tag{A11}$$

Once 4 velocities are measured, the output matrix $\mathbf{C}_a$ takes the following form

$$\mathbf{C}_a = \begin{bmatrix} 0 & 0 & C_{1,3} & C_{1,4} & 0 & 0 & 0 & 0 & 0 & C_{1,10} & 0 & C_{1,12} & 0 & C_{1,14} & 0 & 0 \\ 0 & 0 & C_{2,3} & C_{2,4} & 0 & 0 & 0 & 0 & 0 & C_{2,10} & 0 & C_{2,12} & 0 & C_{2,14} & 0 & 0 \\ 0 & 0 & 0 & 0 & 0 & C_{3,6} & 0 & 0 & 0 & 0 & 0 & 0 & 0 & 0 & 0 & 0 \\ 0 & 0 & 0 & 0 & 0 & 0 & 0 & C_{4,8} & 0 & 0 & 0 & 0 & 0 & 0 & 0 & 0 \end{bmatrix} \tag{A12}$$

where $C_{1,3} = 1$, $C_{1,4} = -(a_2 + b_2)$, $C_{1,10} = Z_1(0)$, $C_{1,12} = Z_2(0)$, $C_{1,14} = Z_3(0)$, $C_{2,3} = 1$, $C_{2,4} = L - a_2 - b_2$, $C_{2,10} = Z_1(L)$, $C_{2,12} = Z_2(L)$, $C_{2,14} = Z_3(L)$, $C_{3,6} = 1$, $C_{4,8} = 1$.

However, if 5 velocities are measured, the output matrix $\mathbf{C}_a$ is offered as follows

$$\mathbf{C}_a = \begin{bmatrix} 0 & 0 & C_{1,3} & C_{1,4} & 0 & 0 & 0 & 0 & 0 & C_{1,10} & 0 & C_{1,12} & 0 & C_{1,14} & 0 & 0 \\ 0 & 0 & C_{2,3} & 0 & 0 & 0 & 0 & 0 & 0 & C_{2,10} & 0 & C_{2,12} & 0 & C_{2,14} & 0 & 0 \\ 0 & 0 & C_{3,3} & C_{3,4} & 0 & 0 & 0 & 0 & 0 & C_{3,10} & 0 & C_{3,12} & 0 & C_{3,14} & 0 & 0 \\ 0 & 0 & 0 & 0 & 0 & C_{4,6} & 0 & 0 & 0 & 0 & 0 & 0 & 0 & 0 & 0 & 0 \\ 0 & 0 & 0 & 0 & 0 & 0 & 0 & C_{5,8} & 0 & 0 & 0 & 0 & 0 & 0 & 0 & 0 \end{bmatrix} \tag{A13}$$

where $C_{1,3} = 1$, $C_{1,4} = -(a_2 + b_2)$, $C_{1,10} = Z_1(0)$, $C_{1,12} = Z_2(0)$, $C_{1,14} = Z_3(0)$, $C_{2,3} = 1$, $C_{2,10} = Z_1(a_2 + b_2)$, $C_{2,12} = Z_2(a_2 + b_2)$, $C_{2,14} = Z_3(a_2 + b_2)$, $C_{3,3} = 1$, $C_{3,4} = L - a_2 - b_2$, $C_{3,10} = Z_1(L)$, $C_{3,12} = Z_2(L)$, $C_{3,14} = Z_3(L)$, $C_{4,6} = 1$, $C_{5,8} = 1$.

Downloaded by [Kungliga Tekniska Hogskola] at 04:36 26 November 2015